

Reconciling single chamber Mg/Ca with whole shell $\delta^{18}\text{O}$ in surface to deep dwelling planktonic foraminifera from the Mozambique Channel

Juliane Steinhardt¹, Caroline Cléroux¹, Lennart Jan de Nooijer¹, Geert-Jan Brummer^{1,2}, Rainer Zahn⁴, Gerald Ganssen², Gert-Jan Reichart^{1,3}

¹ Department of Geology and Chemical Oceanography, NIOZ Royal Netherlands Institute for Sea Research, P.O. Box 59, NL-1790 AB Den Burg, Netherlands, * juliane.steinhardt@nioz.nl

² Faculty of Earth- and Life Sciences, VU University Amsterdam, de Boelelaan 1085, 1081 HV Amsterdam, The Netherlands

³ Department of Earth Sciences, Faculty of Geosciences, Utrecht University, P.O. Box 80021, 3508TA Utrecht, The Netherlands

⁴ Institució Catalana de Recerca i Estudis Avançats (ICREA) and Institut de Ciència i Tecnologia Ambientals, Departament de Física, Universitat Autònoma de Barcelona, Cerdanyola del Vallès, Spain.

Corresponding author: juliane.steinhardt@nioz.nl

Abstract

Most planktonic foraminifera migrate vertically through the water column during life, meeting a range of depth-related conditions as they grow and calcify. For reconstructing past ocean conditions from geochemical signals recorded in their shells it is therefore necessary to know vertical habitat preferences. Species with a shallow habitat and limited vertical migration will reflect conditions of the surface mixed layer and short- and meso-scale (i.e. seasonal) perturbations therein. Species spanning a wider range of depth habitats, however, will contain a more heterogeneous, intra-specimen variability (e.g. Mg/Ca and $\delta^{18}\text{O}$), which is less for species calcifying below the thermocline. Obtained single-chamber Mg/Ca are combined with single specimen $\delta^{18}\text{O}$ and $\delta^{13}\text{C}$ of the surface water inhabitant *Globigerinoides ruber*, the thermocline-dwelling *Neogloboquadrina dutertrei* and *Pulleniatina obliquiloculata* and the deep dweller *Globorotalia scitula* from the Mozambique Channel. Species-specific Mg/Ca, $\delta^{13}\text{C}$ and $\delta^{18}\text{O}$ data combined with a depth-resolved mass balance model confirm distinctive migration and calcification patterns for each species as a function of hydrography. Whereas single specimen $\delta^{18}\text{O}$ rarely reflect changes in depth habitat related to hydrography (e.g. temperature), measured Mg/Ca of the last chambers can only be explained by active migration in response to changes in temperature stratification. Foraminiferal geochemistry and modeled depth habitats shows that the single chamber Mg/Ca and single shell $\delta^{18}\text{O}$ are in agreement with each other and in line with the changes in hydrography induced by eddies.

1. Introduction

Most planktonic foraminifera inhabit the upper 200 meters of the water column, with exceptions of some species living as deep as 1000 m (e.g. Hemleben, 1989). The average depth habitat of individual species and the range of water depths at which they are found reflect their ecology (e.g. feeding behavior), ontogeny and seasonal preferences. Stable oxygen isotope values ($\delta^{18}\text{O}$) and Mg/Ca ratios (Shackleton et al., 1974; Fairbanks et al., 1980; Ortiz et al., 1996; Elderfield and Ganssen, 2000) have been used to reconstruct upper water column conditions using species with a known depth range (e.g. Ravelo et al., 1992; Patrick and Thunell, 1997; Faul et al., 2000; Cl  roux et al., 2013). For many species, however, application of Mg/Ca as a seawater temperature proxy is complicated by depth migration as a function of ontogeny. Previous studies revealed major Mg/Ca heterogeneity within foraminiferal shells (e.g. Eggins et al., 2003; Hathorne et al., 2009; Kunioka et al., 2006; Jonkers et al., 2012), which were attributed to a combination of vertical migration during their life and vital effects. Nevertheless, species-specific patterns of vertical migration and hence depth of calcification determine what part of the water column can be reconstructed.

Field observations show that most foraminiferal species do not occupy a single depth, but rather calcify at a range of depths. Many species migrate vertically as they grow and, therefore, the chemical composition (e.g. Mg/Ca and $\delta^{18}\text{O}$) of their shells changes with age. Fairbanks et al. (1982) and Field (2004) suggested that foraminifera may modify their habitat depth depending on hydrographic condition and food supply. However, little is known about the exact controls on depth habitat, termination of shell growth and controls on shell features (e.g. formation of crusts). A better understanding of the vertical calcification pattern of different species is needed to reconstruct past changes in vertical structure of the water column by using geochemical proxies, e.g. for temperature ($\delta^{18}\text{O}$ and Mg/Ca). Using geochemical signals of species with different and well-constrained calcification depths (Emiliani, 1954; Mulitza et al., 1997) changes in water column conditions can be resolved.

Using core top samples from the Indian Ocean, Birch et al. (2013) report $\delta^{13}\text{C}$ and $\delta^{18}\text{O}$ measurements made on several species of planktonic foraminifera across a range of tightly constrained size windows. From size controlled $\delta^{18}\text{O}$ calcite trajectories they inferred depth habitats, using modern vertical temperature profiles. However, by using multiple core-top specimens this data set encompasses not only vertical changes in the water column structure, but also inter- and intra-annual changes therein, which are both known to vary substantially in this region (e.g. McClanahan, 1988; Damassa et al., 2006; Hastenrath et al., 1993). In this study we

use sediment trap samples, allowing analyses of specimens that lived during a confined time interval and link in situ hydrographic changes (i.e. temperature) more directly to their shell chemistry.

Single-chamber Mg/Ca compositions from specimens with contrasting calcification depths (the surface-dweller *Globigerinoides ruber* (d' Orbigny, 1839), the thermocline-dwelling species *Neogloboquadrina dutertrei* (d' Orbigny, 1839) and *Pulleniatina obliquiloculata* (Parker et al., 1865) and the deep dweller *Globorotalia scitula* (Brady, 1882) reflect temperatures throughout the upper 500 m and were shown to reliably reflect short-term hydrographic changes (Steinhardt et al., 2014). Meso-scale eddies such as observed in the Mozambique Channel (MC) induce variations in temperature and salinity. Anticyclonic (anti-clockwise) eddies in the MC are characterized by a warm water core and are associated with elevated sea surface heights and large vertical isopycnal excursions. Foraminifera living in the mixed layer of the MC are affected by eddy-induced changes, which is reflected by the geochemistry of *G. ruber* and *N. dutertrei* (Steinhardt et al., 2014), resulting in higher Mg/Ca ratios and more depleted $\delta^{18}\text{O}_{\text{cc}}$ values. These short-term changes in vertical water column temperature and $\delta^{18}\text{O}_{\text{sw}}$ distribution should influence shell $\delta^{18}\text{O}$ and Mg/Ca throughout the different ontogenetic stages for any species migrating during its life. Alternatively, foraminifera may respond to altered hydrographic conditions by changing their calcification depth. Here we present combined single-specimen $\delta^{18}\text{O}$ and single-chamber Mg/Ca measurements for different species, providing a composite of thermocline and sub-thermocline conditions. Since single chamber Mg/Ca values cannot be compared one-on-one with whole shell $\delta^{18}\text{O}$ -values we evaluate our results using a mass balance model for depth related carbonate addition of four species of planktonic foraminifera.

2. Oceanographic setting

In the oligotrophic Mozambique Channel (MC) (Fig. 1) sea surface temperatures (SST) vary seasonally and with eddy-induced transport (Fallet et al., 2011). The SSTs range from 25°C to over 30°C with an annual mean of 27.6°C, the seasonal change in temperatures is associated with the monsoon system. With the onset of Austral summer rainfall increases, caused by the seasonal migration of the ITCZ and sea surface salinities decrease slightly from 35.2 in winter to 34.9 in summer (Fallet et al., 2010). The calcite compensation depth in the Western Indian Ocean is below 3000 meters and hence does not result in dissolution of foraminiferal calcite at the depth of the trap's location (2225 m). Southward migration of anticyclonic meso-scale eddies, originating at 10°S north off the Comoros Islands, affects the hydrography in the MC (Fig. 1). Eddies pass

through the MC at a mean frequency of about four to seven per year (at a southward propagation speed of 3-6 km.d⁻¹) before joining the Agulhas Current. An eddy passage is associated with vertical movement of isopycnals, which can occasionally exceed 40 m per day in the upper layer (Ullgren et al., 2012). The formation of meso-scale eddies in the Mozambique Channel is related to variability in the South Equatorial Current (SEC) transport (Backeberg and Reason, 2010; Fig. 1). The main water masses contributing to the upper part of the MC include the Tropical Surface Water (TSW), Subtropical Surface Water (STSW) and Indonesian Throughflow Water (ITFW). The warm, fresh surface water (TSW) forms at equatorial latitudes and is transported westward within or north of the SEC (New et al., 2007). In the proximity of the western margin, where the SEC bifurcates, warm surface waters are transported poleward, either east of Madagascar, or through the MC (e.g. Gründlingh, 1995; Swallow et al., 1988). The STSW is characterized by relatively high salinities and a subsurface maximum, with salinities of 35.2 – 35.5, at approximately 200 m below sea surface, at which depth the surface water subducts below the fresher TSW (Wyrki, 1973).

3. Material & Methods

3.1 Sediment trap and mooring array

Within the Long-term Ocean Climate Observations (LOCO) program, an array of eight moorings across the narrowest part of the Mozambique Channel, provides continuous measurements of current velocities, temperatures and salinities at fixed depths since November 2003 (Ullgren et al., 2012). Sediment traps of the type Technicap PPS 5 were deployed at 16.8°S and 40.8°E in the central MC (Fig. 1), equipped with an automated sampling carousel of 24 cups and a baffled collecting area of 1.0 m². The trap was positioned 250 m above the channel floor at 2250 m water depth. Between November 2003 and February 2009, a total of four sediment trap deployments took place, each programmed to a 17, 21 or 23 days sampling interval. Prior to deployments, sample cups were filled with an HgCl₂-poisoned and borax-buffered solution of seawater collected from the deployments depth (Lončarić et al., 2007). Sediment trap samples were wet-split, sieved and foraminiferal shells were cleaned according to the protocol of Barker et al. (2003), modified by Fallet et al. (2009) (see also Fallet et al., 2010; Steinhardt et al., 2014 for detailed description of the procedure here).

Using sediment trap material allows linking the chemistry of the shells to recorded *in situ* conditions from the moorings and from real-time satellite derived observations. Therefore we are able to link short-term changes in hydrography (i.e. eddies) to the differences in shell chemistry. Calculated back trajectories, based on a high-resolution INALT01 model (Durgadoo et al., 2013), show that

specimens ending up in the sediment trap all originate from the area under influence of the eddy-variability (Steinhardt et al., 2014). We selected the sediment trap intervals during which the complete sediment cup collection took place under either full eddy or full non-eddy conditions (for full description see Steinhardt et al., 2014; supplement). For the selected collecting intervals, temperature and salinity observations from the mooring (Imc5a) are compiled and daily means were used to calculate eddy and non-eddy depth-resolved temperature profiles.

3.2 Temperature and Salinity data

For this study, we used temperatures recorded at 110 m; 200 m and 400 m water depth by a CTD deployed on mooring Imc5A (16.8°S, 41.1°E, Fig. 1), which is closest to the sediment trap site. Moored salinity and temperature data, collected during the selected intervals of eddy and non-eddy conditions (Table S1 in the Supplement), was spline fitted in Analyseries 1.1.6 68K to achieve meter-wise data resolution. Sea surface temperatures were retrieved from the 4 km daytime MODIS/AQUA dataset around trap site (16 – 17°S and 40 – 41°E) for the period of the selected collecting intervals (<http://poet.jpl.nasa.gov/>). Surface salinity data is not available for the complete deployment period and therefore, CTD-based salinity-depth profiles taken during the deployment/recovery cruises were used instead (Ullgren et al., 2012). Based on the trend observed in the moored salinity data at 110 m water depth (Ullgren et al., 2012; less saline during eddy condition) we used CTD minimum surface salinities to represent eddy surface salinities and maximum surface salinities to represent non-eddy conditions. Since salinity mooring data were not available for depths between 400 and 1525 m, we have chosen two more "anchor points" at 700 and 1000 m water depth from the CTD depth profiles in order to better capture the Red Sea Water (RSW) advection at these depths and to achieve a more accurate salinity fitting curve for the upper 1000 m.

3.3 Planktonic foraminiferal species and ontogeny

We selected four species from the sediment trap samples according to differences in depth habitats as reported in previous studies. *Globigerinoides ruber* (white) is a shallow, surface mixed layer dwelling species, occupying the upper 50 m of the water column and is commonly used to reconstruct SST (Hemleben et al., 1989). To minimize a potential biases in $\delta^{18}\text{O}$ and Mg/Ca associated when combining different morphotypes (Steinke et al., 2005), we used only *G. ruber* sensu stricto that was by far the most abundant in these samples (Fallet et al., 2010).

The subsurface-dwellers *Neogloboquadrina dutertrei* and *Pulleniatina obliquiloculata* have been associated with a calcification depth of 0 - 100 meters and 60 - 150 meters in the upper and middle

thermocline, respectively (Erez and Honjo, 1981; Fairbanks et al., 1982; Ravelo and Fairbanks, 1992; Spero et al., 2003; Field, 2004; Kuroyanagi and Kawahata, 2004; Huang et al., 2008). The deep-dwelling species *Globorotalia scitula* was used as a representative for deep water conditions (Bé, 1969; Ortiz et al., 1996; Itou et al., 2001; Fallet et al., 2011).

Measurements on *G. ruber* were usually performed on specimens in the 250 - 315 μm size fraction. In a limited number of samples, abundances of this species were low in this size fraction, and geochemical analyses were therefore performed on specimens from a larger size fraction (315 - 400 μm). Analyses on *N. dutertrei*, *P. obliquiloculata* and *G. scitula* were generally done on the size range >315 μm , with additional measurements on the 250 - 315 μm size fraction depending on the specimen's abundance within a sample. All specimens show excellent preservation and do not show any signs of diagenesis (based on SEM microscopy). Recently, Fallet et al. (2012) showed that shell size normalized weights of three species of planktonic foraminifera from the same sediment trap location do not differ from those of the surface sediment samples below this trap. Absence of dissolution is also reported by Birch et al. (2013) describing planktonic foraminifera from surface sediments at ~ 3000 m water depth, in the northern part of the Mozambique Channel, as being glassy and preserved excellently.

3.4 Mg/Ca and Stable isotope analyses

The Mg/Ca ratios of single chambers used in this study were previously published (Steinhardt et al., 2014) and were determined by Laser Ablation-Inductively Coupled Plasma-Mass Spectrometry (LA-ICP-MS) at Utrecht University (Reichart et al., 2003) (for summary of the results see Tab. 1). Subsequently, specimens were analyzed for whole shell $\delta^{18}\text{O}$ and $\delta^{13}\text{C}$ after removal from the laser ablation stub with ethanol and inspection for possible contaminations. Measurements were performed at the Universitat Autònoma de Barcelona on a Thermo Finnigan MAT253 mass spectrometer coupled to a Kiel IV device for CO_2 sample gas preparation. External reproducibility (1σ) of $\delta^{13}\text{C}$ standards NBS19 and IAEA-CO was 0.04‰ and for $\delta^{18}\text{O}$ 0.08‰.

Single shells from part of the sample set were analyzed using a Thermo Finnigan Delta Plus mass spectrometer equipped with a Gas Bench II preparation device at the VU University Amsterdam. Single specimens were loaded into round-bottom vials, which were subsequently flushed with He. The samples then reacted with phosphoric acid (H_3PO_4) injected into the vial producing CO_2 gas, which is transported in a helium stream to the mass spectrometer. Traps are used to remove residual H_2O from the sample gas and the CO_2 is separated from other possible contaminant gases on a poraplot Q GC column. Reproducibility (1σ) of $\delta^{13}\text{C}$ standards NBS19 and was 0.07‰ and 0.12‰ for $\delta^{18}\text{O}$. Values measured on the Kiel IV and the GASBENCH-II are comparable and

species-specific $\delta^{18}\text{O}_{\text{CC}}$ are in good agreement (Tab. 2). Measurements with the GASBENCH-II have a somewhat wider standard deviation inherent to continuous flow mass spectrometry. In total, 391 single shell stable isotope values were obtained. Values deviating more than twice the standard deviation from the average of the total dataset were regarded as outliers ($n=23$) and removed from the dataset (Tab. S3).

The $\delta^{18}\text{O}_{\text{sw}}$, expressed on the SMOW scale is converted to Pee Dee Belemnite (PDB) scale by subtracting 0.27‰ (Hut, 1987). Various $\delta^{18}\text{O}$ -temperature equations have been proposed and discussed in detail in other studies (Bemis et al., 1998; Regenberg et al., 2009), without clear consensus on the most appropriate equation. Here, we integrated calcification depth for each species calculated by matching the foraminiferal calcite $\delta^{18}\text{O}_{\text{CC}}$ with the calculated calcite $\delta^{18}\text{O}_{\text{calc}}$ following equation (1) from Kim and O'Neil (1997) for the temperature dependent fractionation of calcite by inorganic precipitation (assuming calcification in equilibrium with the ambient seawater).

$$(1) \delta^{18}\text{O}_{\text{eq}} = 25.778 - 3.333 \times \sqrt{43.704 + T} + (\delta^{18}\text{O}_{\text{sw}} - 0.27)$$

We extracted $\delta^{18}\text{O}_{\text{sw}}$ values from the South Indian Ocean for the upper 2000 m (4.5 - 120.2°E; 0 - 32.9°S, $N=154$) from the Global Seawater Oxygen-18 Database (see supplementary table, <http://data.giss.nasa.gov/o18data/>). Additionally we included in situ $\delta^{18}\text{O}_{\text{sw}}$ measurements from the MC, near the sediment trap location (41.08°E; 16.74°S) in order to determine the regional relationship between $\delta^{18}\text{O}_{\text{sw}}$ and salinity (Eq. 2)

$$(2) S = 0.463 * \delta^{18}\text{O}_{\text{sw}} - 15.9, r^2 = 0.87$$

This linear relationship (3) is subsequently used to estimate $\delta^{18}\text{O}_{\text{sw}}$ values based on salinities measured in the proximity of the trap by moored T-S sensors during eddy and non-eddy conditions for depths ranging from 0 to 1000 m.

Seawater temperature and estimated $\delta^{18}\text{O}_{\text{sw}}$ profiles for eddy or non-eddy conditions are used to compare the $\delta^{18}\text{O}$ data depending on the time interval sampled by the sediment trap. We used averaged $\delta^{18}\text{O}_{\text{sw}}$ from the depth range suggested by previously measured single chamber Mg/Ca analyses (Steinhardt et al., 2014), to calculate the $\delta^{18}\text{O}$ -derived calcification temperature for all species, following the temperature equation of Kim and O'Neil (1997):

$$(3) T = 16.1 - 4.64 * (\delta^{18}\text{O}_{\text{CC}} - (\delta^{18}\text{O}_{\text{sw}} - 0.27)) + 0.09 * (\delta^{18}\text{O}_{\text{CC}} - (\delta^{18}\text{O}_{\text{sw}} - 0.27))^2$$

1 The temperature equation of Kim and O'Neil (1997) is the most general calibration, which allows
2 comparing inter specific differences that are automatically accounted for when using species-
3 specific calibrations.

4

5 **4. Results**

6 **4.1 Oxygen isotopes**

7 Single specimen values of $\delta^{18}\text{O}_{\text{CC}}$ range from -3.50‰ to 2.65‰ . Although the values measured
8 on individual specimens clearly overlap, each species has a different average $\delta^{18}\text{O}_{\text{CC}}$ and $\delta^{13}\text{C}_{\text{CC}}$
9 (Fig. 2 and 3). The $\delta^{18}\text{O}_{\text{CC}}$ values are most depleted for *G. ruber*, somewhat more enriched in
10 comparison to *G. ruber* for *P. obliquiloculata* and *N. dutertrei*, with most enriched values in *G.*
11 *scitula* (Tab. 1, Fig. 2 and 3). The relationship between temperature and $\delta^{18}\text{O}_{\text{CC}}$ is generally
12 described with more depleted $\delta^{18}\text{O}_{\text{CC}}$ values indicating higher temperatures and thereby shallower
13 calcification depths. Thus, each species has a distinct whole shell- $\delta^{18}\text{O}$ signature, reflecting their
14 different mean calcification depth. *G. ruber* ($-2.57\pm 0.04\text{‰}$, SD: $\pm 0.24\text{‰}$), *N. dutertrei* and *P.*
15 *obliquiloculata* record negative $\delta^{18}\text{O}_{\text{CC}}$ values between $-1.53\pm 0.03\text{‰}$ (standard deviation (SD): $\pm 0.$
16 42‰) and $-1.13\pm 0.04\text{‰}$ (SD: $\pm 0.24\text{‰}$), more noticeable positive values are found for *G. scitula*
17 with $1.47\pm 0.14\text{‰}$ (SD: $\pm 0.87\text{‰}$) (Fig. 3). No significant trend between size fractions and stable
18 isotopes was observed for any of the analyzed species over the size range we used, as confirmed
19 by ANOVA tests (Kruskal-Wallis one way analysis of variance on ranks) of $\delta^{18}\text{O}_{\text{CC}}$ between the
20 size fractions (*G. ruber*: $p= 0.774$, *N. dutertrei*: $p= 0.500$, *G. scitula*: $p= 0.373$).

21 No significant differences in $\delta^{18}\text{O}$ values for *G. ruber* and *N. dutertrei* were found between eddy
22 and non-eddy conditions. In the deeper dwelling species *P. obliquiloculata* ($U=54$, $P=0.04$) and *G.*
23 *scitula* ($U=80$, $P=0.021$), most depleted $\delta^{18}\text{O}$ values were found during eddy conditions and non-
24 eddy conditions, respectively (Tab. 3; Fig. 3).

25

26 **4.2 Carbon isotopes**

27 Values for $\delta^{13}\text{C}$ range from -1.5‰ to 2.0‰ . Most enriched $\delta^{13}\text{C}$ values are found in *N. dutertrei*
28 ($\delta^{13}\text{C}= 0.53\pm 0.042\text{‰}$, SD: $\pm 0.44\text{‰}$), whereas values for *P. obliquiloculata* are most depleted
29 ($\delta^{13}\text{C}= 0.04\pm 0.04\text{‰}$, SD: $\pm 0.21\text{‰}$). Individuals of *G. ruber* reflect a relatively large range in $\delta^{13}\text{C}_{\text{CC}}$
30 values ($0.51\pm 0.04\text{‰}$, SD: $\pm 0.47\text{‰}$), whereas *G. scitula* ($0.27\pm 0.04\text{‰}$, SD: $\pm 0.22\text{‰}$) displays a
31 much more limited variability in $\delta^{13}\text{C}_{\text{CC}}$ (Tab. 1, Fig. 3). Species specific $\delta^{13}\text{C}$ - $\delta^{18}\text{O}$ relationships
32 (Fig. 2) differ and only *G. scitula* showed a positive correlation between single specimen carbon
33 and oxygen isotope ratios (Fig. 2, $r^2=0.388$, $p<0.001$). Moreover, values for *G. scitula* differ from

34 those of other species, with relatively depleted $\delta^{13}\text{C}$ (0.27‰, SD: $\pm 0.22\%$) and relatively enriched
35 $\delta^{18}\text{O}$ values (1.47‰, SD: $\pm 0.87\%$).

36 From the four investigated species, only *G. scitula* (N: 37) did not show a significant difference in
37 $\delta^{13}\text{C}$ between eddy and non-eddy conditions. *G. ruber* (N: 200; Mann-Whitney rank sum test U=
38 3373, $p = 0.002$), and *P. obliquiloculata* (N: 33; U= 52, $p = 0.032$) showed significantly more
39 positive $\delta^{13}\text{C}$ values during non-eddy conditions. During non-eddy condition however, *N. dutertrei*
40 (N: 118; U= 939.5, $p = 0.002$) recorded more negative $\delta^{13}\text{C}$ values (Fig. 3).

41

42 **4.3 Calcification temperatures**

43 The calculated multi-specimen $\delta^{18}\text{O}$ -based temperature from eq. (3) and the single chamber
44 Mg/Ca are positively, exponentially correlated (Fig. 4). Variability in this relationship is highest at
45 higher ($> 25^\circ\text{C}$) temperatures. Mg/Ca-derived calcification temperatures, for *G. ruber* are on
46 average $28.1 \pm 2.8^\circ\text{C}$, based on the calibration of Fallet et al. (2010) for this species in this region.
47 Calcification temperatures for *N. dutertrei* and *P. obliquiloculata* are $22.5 \pm 3.7^\circ\text{C}$ and $21.6 \pm 3.1^\circ\text{C}$,
48 respectively, both based on species-specific calibrations from Anand et al. (2003). Mg/Ca ratios
49 of *G. scitula* were transformed into temperatures using the equation for *G. hirsuta* (Anand et al.,
50 2003) resulting in an average temperature of $14.4 \pm 3.4^\circ\text{C}$ (Fig. 5). Calcification temperatures
51 based on $\delta^{18}\text{O}$ result in markedly different values, ranging from $29.4 \pm 1.3^\circ\text{C}$ for *G. ruber* to
52 $24.4 \pm 2^\circ\text{C}$ for *N. dutertrei*, $22.5 \pm 1.1^\circ\text{C}$, for *P. obliquiloculata* and $10.4 \pm 3.9^\circ\text{C}$ for *G. scitula* (Tab. 1).
53 Since *P. obliquiloculata* and *G. scitula* showed significant differences for $\delta^{18}\text{O}_{\text{CC}}$ between eddy
54 and non-eddy conditions, we separately calculated temperatures for eddy and non-eddy condition.
55 Mean $\delta^{18}\text{O}$ from Eq. (3) for eddy intervals yield $22.8 \pm 0.9^\circ\text{C}$ for *P. obliquiloculata* and $7.9 \pm 2.1^\circ\text{C}$
56 for *G. scitula*. For non-eddy intervals calcification temperatures are $22.5 \pm 1.2^\circ\text{C}$ for *P.*
57 *obliquiloculata* and $11.8 \pm 4.1^\circ\text{C}$ for *G. scitula* (Fig. 5).

58

59 **5. Discussion:**

60 **5.1 Single specimen isotope temperatures**

61 The average, single-specimen $\delta^{18}\text{O}_{\text{CC}}$ of *G. ruber* reflect SSTs of $27.0 \pm 2.2^\circ\text{C}$ - $28.4 \pm 2.1^\circ\text{C}$ (based
62 on sediment-trap calibrations from Fallet et al., 2010 and Wilke et al., 2009, respectively), which
63 is close to the satellite-derived annual mean SST of 27.6°C (Fallet et al., 2010). When applying
64 the equation of Kim and O'Neil (1997) for conversion of $\delta^{18}\text{O}_{\text{CC}}$ into temperature SST is
65 considerably higher ($29.4 \pm 1.3^\circ\text{C}$). This discrepancy, may be caused by the fact that the calcite-
66 water calibration of Kim and O'Neil (1997) is based on inorganic precipitation experiments, free of

67 vital effects and therefore may be offset compared to the temperature- $\delta^{18}\text{O}_{\text{CC}}$ relationship of
68 biogenic carbonates. Nevertheless this temperature estimate based on Kim and O'Neil (1997) is
69 in good agreement with the average temperature of $28\pm 1.1^\circ\text{C}$ during the investigated intervals.
70 The intertest variability of this species can be explained by the high temperature variability at the
71 sea surface, as well as differences in symbiont activity. The shallow depth habitat of *G. ruber* in
72 the MC is in line with previous studies showing that this species is confined to the photic zone
73 (e.g. Deuser et al., 1981; Lončarić et al., 2006; Peeters and Brummer, 2002), because of the light
74 requirement of its symbionts. Based on its relatively narrow preferred depth habitat, this species
75 is a suitable tracer for (sub)tropical surface-water (0 - 100 meters, mixed layer) conditions (e.g.
76 Deuser, 1987; Anand et al., 2003; Field, 2004; Fallet et al., 2010). Birch et al. (2013) show that
77 shell size of specimens of *G. ruber* is not correlated to $\delta^{18}\text{O}_{\text{CC}}$, confirming that this species
78 occupies a narrow calcification depth during its life. In addition to its shallow living depth, *G. ruber*
79 is known to occur in some areas relatively equally throughout the year (e.g. Deuser, 1987; Mohtadi
80 et al., 2006; Tedesco et al., 2007), whereas in other areas, including the MC, they occur at highest
81 densities during summer months (e.g. Tolderlund and Bé, 1971; Duplessy et al., 1981; Ganssen
82 and Sarnthein, 1983; Deuser and Ross, 1989; Eguchi et al., 2003; Lončarić et al., 2006; Fallet et
83 al., 2010). This seasonal preference results in SSTs that are slightly biased towards summer
84 conditions when using fossil specimens of this species.

85
86 Based on an average $\delta^{18}\text{O}_{\text{CC}}$ -derived temperature of $24.3\pm 2^\circ\text{C}$ (Tab. 2), following the equation of
87 Kim and O'Neil (1997), calcification depths of *N. dutertrei* are in the range of 20 - 130 m (Fig. 6)
88 with an average of 58 m. For eddy conditions, the average calcification depth is approximately 80
89 m, for non-eddy condition it is approximately 37 m. Average Mg/Ca-based temperature of
90 $22.5\pm 4^\circ\text{C}$ is in relatively good agreement with the average $\delta^{18}\text{O}_{\text{CC}}$ -derived temperature (Tab. 2).
91 The difference between Mg/Ca- and $\delta^{18}\text{O}$ -based temperatures are smaller than the 1.2°C
92 uncertainty associated with the Mg/Ca calibration (Anand et al., 2003). Previous studies using *N.*
93 *dutertrei* from Indian Ocean core top samples and Mozambique Channel sediment traps have
94 reported similar depth ranges between 40 - 150 m (Kiefer et al., 2006) and similar average depths
95 of 80 m (Fallet et al., 2011), respectively. Both of these studies used pooled specimens for their
96 stable isotope analysis and hence provided the population's average calcification depth.
97 Moreover, pooling of specimens from sediment core samples (Kiefer et al., 2006) does not allow
98 for resolving short-term variability in calcification temperatures as do single specimens (e.g.
99 seasonality). The inferred calcification depth for *N. dutertrei* is in line with its characterization as
100 an intermediate deep dwelling species, living preferentially in the seasonal thermocline (e.g.

101 Fairbanks et al., 1982; Curry et al., 1983; Eguchi et al., 2003; Farmer et al., 2007), coinciding with
102 a deep chlorophyll maximum (Fairbanks et al., 1980; Ravelo et al., 1990). Overall living depth of
103 this species is confined to the upper 200 m (Farmer et al., 2007; Kroon and Darling, 1995).
104 Variability in Mg/Ca within single specimen shell walls of *N. dutertrei* from the Timor Sea
105 suggested temperatures between 12 and 23°C, implying migration through the entire thermocline
106 (Eggins et al., 2003). However, most calcification seems limited to a much smaller depth interval
107 and the extremes in Mg/Ca might reflect upper and lower depth limits occupied by this species.
108 Moreover, banding of Mg/Ca in shell calcite has been viewed in terms of discrete calcification
109 events (Elderfield et al., 1996; Erez et al., 2003). Plankton tow studies (Fairbanks et al., 1980)
110 showed oxygen isotope equilibrium calcification for *N. dutertrei* and *P. obliquiloculata*.

111
112 The $\delta^{18}\text{O}_{\text{CC}}$ -based calcification depths for *P. obliquiloculata* reported here (48-125 m, with an
113 average of 74 m, Fig. 6) are in close agreement with those reported previously (e.g. between 60
114 and 80 m; Mohtadi et al., 2009). Indeed, in plankton tows from the central equatorial Pacific the
115 largest abundance of adult *P. obliquiloculata* with a terminal cortex was found below 60 m (Watkins
116 et al., 1996). All specimens used in this study had the distinctive smooth outer cortex that envelops
117 the final whorl in the adult as well as an arched aperture (Watkins et al., 1996). Non-corticated *P.*
118 *obliquiloculata* (“juveniles”) are confined mostly to the mixed layer (Watkins et al., 1996), indicating
119 migration to greater depths at the time of cortex formation during the terminal stage of its life cycle
120 (Erez and Honjo, 1981; Hemleben et al., 1989; Ravelo and Fairbanks, 1992).

121 The average $\delta^{18}\text{O}_{\text{CC}}$ for *G. scitula* yields a calcification temperature of $10.4 \pm 3.9^\circ\text{C}$, suggesting that
122 this species calcifies between 290 and 1100 m (Fig. 6) with an average of approximately 500 m.
123 This overlaps with the depth range indicated by the Mg/Ca temperatures of $14.4 \pm 3.4^\circ\text{C}$ derived
124 from the last few chambers added, suggesting that these shells formed at a depth between about
125 250 and 350 meter for non-eddy and eddy conditions respectively. The $\delta^{18}\text{O}_{\text{CC}}$ based estimates,
126 however, do not consider possible vital effects that were previously suggested for this species
127 (e.g. Kahn and Williams, 1981). If taken into account, this would lower the temperature and depth
128 habitat estimates by some 4°C and 500 m, respectively.

129 Birch et al. (2013) support previous findings of a distinct positive correlation between $\delta^{18}\text{O}$ and
130 size in *G. scitula* (e.g. Friedrich et al., 2012), which is linked to a substantial ontogenetic vertical
131 migration through the water column. Largest individuals have been inferred to live below the
132 thermocline, consistent with the supposed absence of symbionts in this species. This is in line
133 with our observations, showing higher inter-specimen variability in $\delta^{18}\text{O}_{\text{CC}}$ for *G. scitula*, than in
134 the other species.

135

136 **5.2 Habitat depth versus calcification depth**

137 Planktonic foraminifera collected by sediment traps might record $\delta^{18}\text{O}_{\text{cc}}$ signals comprising
138 calcification at various depths and thus document an *apparent* average calcification depth by
139 integrating the entire calcification history of the specimen. Given changes in seawater temperature
140 with water depth, even minor changes in the upper or lower range of the depth at which planktonic
141 species calcify, can have a profound effect on the average $\delta^{18}\text{O}_{\text{cc}}$ and reconstructed temperature.
142 Since evidence is accumulating that some species have a flexible calcification range (e.g. due to
143 seasonality or local hydrography; Lončarić et al., 2006; Wilke et al., 2009), interpretation of down
144 core stable isotope data in terms of thermal structure may be challenging. Therefore, it is crucial
145 to accurately quantify the impact of environmental factors on depth preferences of planktonic
146 foraminifera. Contrasting eddy and non-eddy conditions, a short-term feature, allow us to
147 disentangle seasonal and other short-term local hydrography changes and their effect on
148 foraminiferal calcification depth.

149 While Mg/Ca-based temperatures of *G. ruber* and *N. dutertrei* record eddy induced changes in
150 upper water column stratification (Steinhardt et al., 2014), $\delta^{18}\text{O}$ -based temperatures are relatively
151 similar for both species (Fig. 6). Using the paleo-temperature equation (equation (1); Kim and
152 O'Neil, 1997) and fitting $\delta^{18}\text{O}_{\text{calc}}$ with $\delta^{18}\text{O}_{\text{cc}}$, we find that *G. ruber* calcifies on average at the sea
153 surface (down to 7 m during non-eddy conditions and down to 18 m under eddy conditions) (Fig.
154 6). *N. dutertrei* calcifies on average between 12 and 120 m during eddy conditions (average
155 calcification depth 81 m) and between 17 and 58 m under non-eddy conditions (average 37 m).
156 During eddy conditions, *P. obliquiloculata* calcifies between 89 and 124 m (average 107 m),
157 whereas it calcifies at shallower depth, between 20 and 77 m (average calcification depth 60 m)
158 during non-eddy condition. Largest changes in calcification depth in this study are inferred from
159 *G. scitula*. From a calcification range between 500 to 1100 m and an average calcification around
160 716 m during eddy condition it shifts to a calcification range from 168 to 745 m and an average
161 calcification depth of 343 m (Fig. 6).

162
163 Conversely, $\delta^{18}\text{O}$ -based temperatures are significantly different for *P. obliquiloculata* and *G.*
164 *scitula*, while the Mg/Ca-based temperature of the last formed chambers of *P. obliquiloculata*
165 indicate similar calcification temperature (Tab. 1). Mg/Ca inferred calcification temperatures,
166 representing the depth occupied at the later stages of the foraminifer's life, were similar between
167 eddy and non-eddy conditions. Nonetheless, temperature mooring data show a steep temperature
168 gradient, coinciding with the habitat depth of *G. scitula*, and thereby revealing a wide range of

169 calcification depths for this species, changing significantly with deepening of the thermocline
170 during eddy passage.

171
172 Inferred higher variability in calcification temperature for *G. ruber* presented in this study compared
173 to observed satellite SST likely results from the spatial resolution employed here. Inter-individual
174 differences in depth migration add to the variability in isotopes and element/Ca ratios when
175 measuring single specimens. Potential effects of ontogeny on stable isotope composition are
176 minimized by using narrow size fractions, as confirmed by the lack of ontogenetic trends with shell
177 size in our measurements. Russell and Spero (2000) concluded that natural variability in oxygen
178 isotopes is species specific. Measuring single specimen $\delta^{18}\text{O}_{\text{cc}}$ of *G. ruber* shells from sediment
179 traps in the eastern equatorial Pacific, they show that over a 1.5 – 3 day period, the standard
180 deviation of $\delta^{18}\text{O}$ results in a temperature variability of $\pm 0.87^\circ\text{C}$. Such a variability could explain
181 between 12 and 38% of the variability in $\delta^{18}\text{O}$ -based temperatures in our samples. Another cause
182 of natural variability might be differences in depth at which an individual calcifies. In laboratory
183 cultures, the addition rate of new chambers in *G. sacculifer* ranges from 1.6 to 6.2 days (Bé, 1981),
184 while chamber formation in *G. hirsuta* and *G. truncatulinoides* takes about 5 to 6 hours (Bé, 1979).
185 Considering that our sample duration ranges between 17 and 21 days, $\delta^{18}\text{O}$ variability is likely to
186 be affected by other parameters (e.g. temperature). Therefore, the observed variability in $\delta^{18}\text{O}$ -
187 based temperatures caused by species specific natural variability in $\delta^{18}\text{O}_{\text{cc}}$ (e.g. Russell and
188 Spero, 2000) during the time it takes to add new chambers, which might be calcified under different
189 conditions or water depth.

190
191 **5.3 Reconciling $\delta^{18}\text{O}$ and Mg/Ca-derived calcification depths**

192 Mg/Ca-derived temperatures indicate that calcification depths of *N. dutertrei* range between 42-
193 169 m (average depth: 81 m) under non-eddy conditions and between 13 and 196 m (average
194 depth: 98 m) during eddy conditions (Steinhardt et al., 2014). Thus, the shoaling in average
195 calcification depth from 98 m during eddy conditions to 81 m during non-eddy conditions, indicated
196 by the whole shell $\delta^{18}\text{O}_{\text{cc}}$ is less as than inferred from Mg/Ca, derived from the calcification of the
197 last chambers. A more pronounced trend is present in Mg/Ca of *P. obliquiloculata*, shifting
198 between 70 and 90 m (average 75 m) during non-eddy conditions, to depths between 147 and
199 244 m (average 150 m) during eddy conditions (Steinhardt et al., 2014). The Mg/Ca-derived shift
200 is hence larger than the shift inferred from $\delta^{18}\text{O}_{\text{cc}}$ (eddy: 107 m and non-eddy: 60 m). Mg/Ca-
201 derived calcification temperatures for *N. dutertrei* and *P. obliquiloculata* are hence cooler and
202 indicative of deeper calcification of the final chambers compared to that of the whole shell (based

203 on $\delta^{18}\text{O}_{\text{cc}}$). Calcification temperatures derived from Mg/Ca for *G. scitula* (Fig. 5), indicate an
204 opposite trend, shifting between approximately 200 and 460 m (average 330 m) during eddy
205 conditions to shallower depths between approximately 120 and 420 m (average 270 m) during
206 non-eddy conditions (Steinhardt et al., 2014). Although the $\delta^{18}\text{O}_{\text{cc}}$ suggests calcification somewhat
207 deeper than the Mg/Ca data, both Mg/Ca and $\delta^{18}\text{O}$ -derived calcification depth indicate a shoaling
208 for this species during non-eddy conditions. Furthermore, the average $\delta^{18}\text{O}$ -derived calcification
209 temperature of $10.4 \pm 3.9^\circ\text{C}$ is in good agreement with previously published results for this species
210 (Fallet et al. 2011; Birch et al. 2013). We refrain from correcting for a vital effect, as this would
211 lower $\delta^{18}\text{O}$ -derived calcification temperature to values unrealistically lower than the Mg/Ca-
212 derived calcification temperatures for the last chambers. The observed remaining offset between
213 single-specimen $\delta^{18}\text{O}$ and single chamber Mg/Ca in *G. scitula* suggest that either 1) there is a vital
214 effect resulting in more enriched (i.e. positive) $\delta^{18}\text{O}$ values than when this species would
215 precipitate its shell in isotopic equilibrium with seawater, 2) a more shallow calcification depth
216 during formation of the final chamber, 3) that crust carbonate adds significantly to the total shell
217 mass, or, 4) the Mg/Ca calibration for *G. hirsuta* (Anand et al., 2003) might be different from that
218 of *G. scitula*. Following the vital effect correction of Williams and Kahn (1981), calcification
219 temperature is $6.4^\circ\text{C} \pm 3.9^\circ\text{C}$, which is equivalent to an average calcification depth for *G. scitula*
220 between 600 and deeper than 1100 m. This is in agreement with a suggested depth habitat within
221 the upper 1000 m for this species (Schiebel et al., 1995; Ortiz et al., 1996; Itou et al., 2001). In our
222 opinion the last two explanations are most likely, however, irrespective of the underlying
223 mechanism it is clear that the majority of the test carbonate precipitated at a depth greater or
224 comparable to that of the ontogenetic carbonate of the final chambers.

225 The range of uncertainties related to a species' average calcification depth results from
226 the relatively large natural inter-specimen variability in Mg/Ca. Since we focus on relative
227 differences within species between hydrographic conditions, the uncertainty in calcification
228 temperature resulting from errors in the applied Mg/Ca-temperature calibration does not affect the
229 absolute temperature differences between the eddy- and non-eddy conditions. Instead,
230 uncertainties in the calculated difference in calcification depths between species will be caused
231 by the inter-specimen variability in Mg/Ca.

232

233 **5.3.1 Cumulative calcification model**

234 We used a conceptual oxygen isotope mass balance model (Wilke, 2006; 2009), applying the
235 temperature fractionation from inorganic calcite precipitation of Kim and O'Neil (1997) to our
236 measured $\delta^{18}\text{O}_{\text{cc}}$. The model equation describing foraminiferal migration as a function of depth

237 used here is known as the cumulative form of the Weibull function (Weibull, 1939). It is a
238 continuous probability function (Eq. 4), relating the shell mass 'M' to depth (z) using two constants
239 (α and β) determining the shape of this relationship:

240

$$241 \quad (4) \quad M(z) = 1 - \exp(-1*(z/\beta)^\alpha)$$

242

243 Since shell size of planktonic foraminifera is thought to increase with water depth (Hemleben and
244 Bijma, 1994; Peeters and Brummer, 2002) shell mass must also increase with depth. The isotopic
245 composition of a single shell thus represents the weighted sum of equilibrium calcite precipitated
246 over a depth range of the productive zone (i.e. where primary calcite formation takes place).

247 Based on equation (5), the expected stable isotope composition of a specimen for a discrete water
248 depth interval can be calculated as follows:

249

$$250 \quad (5) \quad \delta^{18}\text{O}_{\text{model}} = \sum_i^n \frac{(M_i - M_{i-1}) + \delta^{18}\text{O}_{\text{eq},i}}{M_i}$$

251

252 Given the $\delta^{18}\text{O}_{\text{eq}}$ profile in the water column and the measured $\delta^{18}\text{O}_{\text{cc}}$ of the planktonic foraminifera
253 it is possible to model the mass development (growth pattern) by using the determined Mg/Ca
254 calcification depth of the last chambers, indicating the base of the calcite production zone. The
255 Mg/Ca-based temperature of the F-1 chamber was used to delimit 95% of the calcite production.
256 In equation (5), $\delta^{18}\text{O}_{\text{eq},i}$ denotes the interval averaged $\delta^{18}\text{O}$ of equilibrium calcite for the specified
257 depth interval. For convenience, shell mass at the sea surface was taken as zero and modelled
258 $\delta^{18}\text{O}_{\text{cc}}$ was done by adapting the variables ' α ' and ' β ' in equation 5.

259 Increasing the value of ' α ' results in a growth curve with a narrow calcification range. Higher values
260 for ' β ' result in a deepening of the growth curve, thereby determining the position of the base of
261 the productive zone. In contrast to Wilke's (Wilke et al., 2006; 2009) approach, we have
262 determined the calcification temperatures of the last three to four chambers, which were used to
263 constrain the base of the calcification range and hence constrained values for ' β '.

264 In this model, it is assumed that shell growth always follows the same function, which is continuous
265 and does not differ between species. Offsets between $\delta^{18}\text{O}_{\text{cc}}$ and $\delta^{18}\text{O}_{\text{sw}}$ from expected
266 equilibrium ('the vital effect'), is assumed to be constant over the temperature range in which the
267 species calcifies. We have adapted $\delta^{18}\text{O}_{\text{sw}}$ in meter steps as calculated from *in situ* salinity
268 measurements, which were interpolated for the upper 2000 meters. We have used expected
269 $\delta^{18}\text{O}_{\text{eq}}$ values of eddy and non-eddy condition to compare depth distributions for all four species
270 of planktonic foraminifera.

271 Calcification depths inferred from the cumulative $\delta^{18}\text{O}$ model (Fig. 7) match previously published
272 calcification depths and associated temperatures for each of the species relatively well (e.g.
273 Cléroux et al., 2008; 2013; Wilke et al., 2009; Fallet et al., 2010; 2011; Birch et al., 2013). In three
274 species, measured $\delta^{18}\text{O}_{\text{CC}}$ values reflect shallower calcification depths than do single-chamber
275 Mg/Ca-based calcification depths, which is consistent with the general model of migration to
276 greater depth during growth. In case of the deep dwelling *G. scitula*, however, $\delta^{18}\text{O}$ -based
277 calcification depth is below that of the final chambers as derived from Mg/Ca-temperatures.
278 Without applying a temperature correction for $\delta^{18}\text{O}$ -based calcification temperatures of *G. scitula*,
279 calcification depth based on $\delta^{18}\text{O}_{\text{CC}}$ can deviate up to 300 m from the Mg/Ca based depths. This
280 would suggest that the majority of the previously formed calcite was precipitated deeper in the
281 water column. The model shows that species modulate their calcification pattern depending on
282 the hydrographical conditions they live in (e.g. eddy, non-eddy condition). For *G. ruber*, our results
283 show that this species seems to be an exclusive surface dweller and hence an application of the
284 cumulative calcification model only confirms that the majority of the calcite is formed at the sea
285 surface.

286 For the thermocline dwelling species *N. dutertrei* we find that this species calcifies most of its
287 calcite in a narrow depth range. Our model indicates that calcification during eddy conditions is
288 more intense in the deeper part of the thermocline ($\alpha= 8.8$; $\beta= 85$), whereas calcification during
289 non-eddy condition is more equally distributed over the entire thermocline ($\alpha= 1.9$; $\beta= 47$). It is
290 noteworthy that *N. dutertrei* appears to intensify its calcification efforts during eddy conditions
291 deeper in the thermocline, matching well with the deepening of the isopycnals and hence a
292 narrower range of optimal calcification conditions (Steinhardt et al., 2014). This calcification
293 response is also reflected in more enriched $\delta^{13}\text{C}$ values during eddy conditions. For *P.*
294 *obliquiloculata* modelled α and β values are relatively high, particularly during eddy conditions ($\alpha=$
295 5.25 ; $\beta= 133$, compared to $\alpha= 3.1$; $\beta= 63$ for non-eddy conditions). This indicates that most of the
296 calcification in *P. obliquiloculata* takes place at a water depth around 125 m during eddy
297 conditions, and around 50 m during non-eddy conditions. The range at which *G. scitula* calcifies
298 is well below the seasonal thermocline, reflected by high values for α and β (Fig. 7) and does not
299 vary considerably during eddy and non-eddy conditions.

300 In general, we conclude that temperature changes within the thermocline induced by eddies affect
301 non-symbiotic species mostly. Also, changes in cumulative calcite addition with depth seem to be
302 species-specific. We modified the model by including Mg/Ca-based temperatures (following the
303 species specific equations of Anand et al., 2003) of the F-1 chamber to constrain the 95%
304 calcification level. This allows to predict expected $\delta^{18}\text{O}_{\text{eq}}$ for different species and shell sizes

305 (Spero et al., 1997; Bijma et al., 1999; Itou et al., 2001; Peeters et al., 2002). The extended version
306 of the model does not distinguish between calcite deposited during chamber formation (primary
307 calcite) and calcite added as a result of wall thickening due to gametogenic calcite or the
308 precipitation of crust (secondary calcite, Bé, 1980; Duplessy et al., 1981; Lohmann, 1995, Jonkers
309 et al., 2012). Secondary calcification might play an important role for deeper dwelling species such
310 as *G. scitula*, which could explain the offset (about 1‰) between $\delta^{18}\text{O}_{\text{model}}$ and $\delta^{18}\text{O}_{\text{CC}}$. This
311 suggests that relatively more calcite is formed deeper in the water column, or secondary calcite is
312 precipitated with a fundamentally different calcification mechanism.

313

314 **5.3.2 Carbon isotopes – testing the calcification model**

315 The $\delta^{13}\text{C}$ values found in planktonic foraminifera is primarily a function of the carbon isotope
316 composition of the dissolved inorganic carbon (DIC) in seawater (e.g. Urey, 1947; Epstein et al.,
317 1953; McCorkle et al., 1990), which changes with water depth (e.g. Fairbanks et al., 1980, Curry
318 and Crowley, 1987). Therefore, we can use the cumulative mass balance model output of the
319 mass added per meter to calculate $\delta^{13}\text{C}_{\text{expect}}$ as the weighted sum of the $\delta^{13}\text{C}_{\text{DIC}}$ (Wilke et al.,
320 2006). Depth-resolved carbon isotope composition ($\delta^{13}\text{C}_{\text{DIC}}$), available from locations closest to
321 our study site (locations between 37-43 °E and 24.7 °S, World Ocean Database 2009) were used
322 to calculate the expected $\delta^{13}\text{C}$ of each species of foraminifera ($\delta^{13}\text{C}_{\text{expect}}$). Since there is no relation
323 between size and stable carbon isotopes in our specimens, the employed size fractions contained
324 only mature (adult) specimens (Brummer et al., 1986, 1987). Comparing water column $\delta^{13}\text{C}_{\text{DIC}}$
325 data (Supplement, Fig. A1) from several stations near the MC reveals that absolute values and
326 depth range over which values decrease is similar at the different sites. To verify the depth related
327 calcification model we compare measured $\delta^{13}\text{C}_{\text{CC}}$ with model-based $\delta^{13}\text{C}_{\text{expect}}$ values (Fig. 8).

328 Carbon isotope values become more negative from surface dwelling *G. ruber* towards deeper
329 dwelling *P. obliquiloculata* near the upper thermocline. Conversely, the $\delta^{13}\text{C}$ of *Globorotalia scitula*
330 increases with depth. Low temperatures and reduced food availability have been suggested to
331 result in relatively low metabolic rates in deep dwelling species, so that their $\delta^{13}\text{C}$ likely approaches
332 $\delta^{13}\text{C}_{\text{DIC}}$ values (Birch et al., 2013). This suggests the involvement of biological controls on the $\delta^{13}\text{C}$
333 of the different genera (*Globigerinoides*, *Neogloboquadrina*, *Pulleniatina* and *Globorotalia*). All
334 $\delta^{13}\text{C}_{\text{expect}}$ are higher than the measured $\delta^{13}\text{C}_{\text{CC}}$.

335 Our cumulative mass balance shows that the majority of the carbonate of *G. ruber* is formed in
336 surface waters (Fig. 7). Equal $\delta^{13}\text{C}_{\text{expect}}$ values for eddy and non-eddy conditions are the result of
337 similarly enriched $\delta^{13}\text{C}_{\text{DIC}}$ in the mixed layer. The measured differences in $\delta^{13}\text{C}_{\text{CC}}$ (Fig. 8) are likely

338 a consequence of the deepening thermocline during passage of an eddy, carrying nutrient-
339 depleted waters (Kolasinski et al., 2013). Anticyclonic eddies are characterized by accumulation
340 of warm, nutrient-poor and chlorophyll-depleted water in the center, which implies that also $\delta^{13}\text{C}_{\text{DIC}}$
341 is more isotopically enriched. Still, local nutrient enrichment potentially occurs at the outer edge
342 as a result of high turbulence along the isopycnal slope (e.g. Falkowski et al., 1991; Lévy, 2003).
343 The strong response of the Mg/Ca and $\delta^{18}\text{O}$ of *N. dutertrei* during eddy conditions (deeper
344 calcification) is also reflected by more depleted $\delta^{13}\text{C}_{\text{CC}}$ values. Remineralization of organic matter
345 at greater depth cause enrichment of $\delta^{13}\text{C}_{\text{DIC}}$, resulting in the incorporation of lighter carbon
346 isotopes into the shell of *N. dutertrei* during eddy conditions. Based on samples from a sediment
347 trap in Cape basin, Wilke et al. (2009) showed that the species *N. dutertrei* is an accurate recorder
348 of the $\delta^{13}\text{C}_{\text{DIC}}$. This is in agreement with previous findings (Mulitza et al., 1999), showing that the
349 carbon isotopic composition of *N. dutertrei* exhibits a constant and temperature-independent off-
350 set from $\delta^{13}\text{C}_{\text{DIC}}$ of $\sim 0.5\text{‰}$ over a wide temperature range. This difference is in line with the offset
351 in our dataset between $\delta^{13}\text{C}_{\text{expect}}$ and $\delta^{13}\text{C}_{\text{CC}}$ of *N. dutertrei* (0.6‰).

352 The $\delta^{13}\text{C}$ of the symbiont-barren *G. scitula* significantly deviates from those of the shallower
353 dwelling species as a result of a decrease in $\delta^{13}\text{C}_{\text{DIC}}$ with water depth (see supplementary
354 information, Fig. A1 and A2). The more depleted $\delta^{13}\text{C}_{\text{CC}}$ of *G. scitula* may also be a consequence
355 of a lower metabolism of this species (Vergnaud-Grazzini, 1976; Kahn, 1977, 1979; Berger et al,
356 1978; Erez, 1978) compared to that of *G. ruber* and *N. dutertrei*. At high metabolic activity, more
357 isotopically lighter carbon is incorporated and since lower temperatures usually reduce metabolic
358 rates, species inhabiting deeper water depths may incorporate relatively heavier carbon isotopes.
359 Minor changes in $\delta^{13}\text{C}_{\text{CC}}$ for *G. scitula* during eddy versus non-eddy conditions are in line with the
360 minor response in calcification depth for this species. Similar to previous conclusions, this
361 suggests that Mg/Ca inferred temperature differences between *N. dutertrei* and *G. scitula* are good
362 indicators for eddies passing (Steinhardt et al., 2014). In addition, the $\delta^{13}\text{C}_{\text{CC}}$ differences between
363 these species might very well help to reconstruct eddy frequency in this area. The depth integrated
364 difference between $\delta^{13}\text{C}$ of *N. dutertrei* and *G. scitula* changes from 0.25 to 0.05 ‰.

365 Comparing $\delta^{13}\text{C}_{\text{expect}}$ and $\delta^{13}\text{C}_{\text{CC}}$ for *P. obliquiloculata* there is a discrepancy between eddy and
366 non-eddy conditions (Fig. 8). Similar to *N. dutertrei*, this species is mostly associated with the
367 thermocline (Anand et al., 2003; Cléroux et al., 2008; Sadekov et al., 2009). Our cumulative
368 calcification model showed a slightly deeper calcification depth for *N. dutertrei* and a minor eddy
369 response in calcification range (Fig. 7). However, $\delta^{13}\text{C}$ values indicate a significant difference
370 between eddy and non-eddy conditions. Mulitza et al. (1999) showed that *P. obliquiloculata* does

371 not calcify in isotopic equilibrium with dissolved ΣCO_2 , but the deviation from isotopic equilibrium
372 is a linear function of temperature (Fig. 8). While the mean of the $\delta^{13}\text{C}$ cannot be used to infer the
373 actual calcification depth, they argue that the spread and skewness of the individual $\delta^{13}\text{C}$
374 measurements should still be representative of the range of calcification depths and habitat
375 preferences within the thermocline.

376 Also changes in the carbonate ion concentration with depth potentially play an important role in
377 the observed differences between species and between eddy and non-eddy conditions
378 (supplementary, Fig. A1 and A2). Since the carbonate ion profile is expected to change in
379 accordance with thermocline deepening when an eddy passes we refrained from correcting for
380 this. The observed offsets between species, however, suggest that carbonate ion does play a role
381 there. The deeper living species show an increasing offset with respect to the 1:1 line (Fig. 8). The
382 exception is *P. obliquiloculata* which responds to temperature rather than $\delta^{13}\text{C}_{\text{DIC}}$ carbonate ion
383 changes (Mulitza et al., 1999).

384 Overall the here observed relations indicate that interpretation of the foraminifera vertical
385 distribution in the upper water column can be unraveled by coupling various geochemical methods
386 in order to retrieve calcification temperature at different stages in a foraminifera's life cycle. This
387 in turn can be used to develop new proxies for the thermal and nutrient structure of the upper part
388 of the water column.

389

390 **6. Conclusion**

391 Documenting changes in upper ocean stratification is essential for understanding past climatic
392 conditions from sediment cores and is commonly estimated by determining the difference in $\delta^{18}\text{O}$
393 between thermocline and surface-dwelling planktonic foraminifera (Spero et al., 2003; Cléroux et
394 al., 2007; Farmer et al., 2007; Lin and Hsieh, 2007; Steph et al., 2009). We conducted stable
395 isotope measurements on four species of planktonic foraminifera (*G. ruber*, *N. dutertrei*, *P.*
396 *obliquiloculata* and *G. scitula*) from selected sediment trap samples, representing eddy and non-
397 eddy conditions in the MC.

398 Using single shell $\delta^{18}\text{O}_{\text{CC}}$ paired to single-chamber LA-ICP-MS Mg/Ca measurements we applied
399 a cumulative mass balance model in order to compare growth patterns of the various planktonic
400 species during eddy and non-eddy conditions. The results indicate that most of the species have
401 somewhat different calcification patterns during eddy and non-eddy conditions. Only Mg/Ca values
402 of *G. scitula* suggest higher calcification temperatures than inferred from $\delta^{18}\text{O}$. Furthermore, the
403 results of the $\delta^{18}\text{O}$ cumulative mass balance model agree with previous findings that thermocline

404 dwelling *N. dutertrei* and deep dwelling *G. scitula* are suitable recorders of eddy induced
405 hydrographic changes (Steinhardt et al., 2014). The combination of various proxies (e.g. Mg/Ca,
406 $\delta^{18}\text{O}$ and $\delta^{13}\text{C}$) can thus provide a useful set of geochemical proxies to reconstruct the thermal
407 and nutrient structure of the upper part of the water column.

408
409 All species analyzed have unique offsets from ambient seawater $\delta^{13}\text{C}$. However, comparison of
410 species specific isotopic trajectories with water column $\delta^{13}\text{C}$ reveals that ambient $\delta^{13}\text{C}_{\text{DIC}}$ may be
411 recorded by the species used in this study. The $\delta^{13}\text{C}$ of *N. dutertrei* and *G. scitula* show eddy
412 related changes in their offsets and can potentially aid to unravel eddy related changes in the
413 nutrient structure.

414

415 **The Supplement related to this article is available online at**
416 **doi:10.5194/bgd-11-17255-2014-supplement.**

417

418 *Acknowledgements.* We acknowledge funding from the European Commission 7th Framework Marie Curie
419 People program FP7/2007–2013 through funding of the Initial Training Network “GATEWAYS”
420 (<http://www.gateways-itn.eu>) under the grant number 238512. Furthermore we acknowledge funding from
421 the LOCO and INATEX programs by the Netherlands Organisation for Scientific Research. Analyses and
422 visualizations of satellite SST used in this paper were produced with the Giovanni online data system,
423 developed and maintained by the NASA GES DISC. We thank the chief scientist Herman Ridderinkhof and
424 the crew of the RRV Charles Darwin, RRV Discovery, FS Meteor, RV Pelagia and R/V Algoa. Great thanks
425 to Helen de Waard and Michiel Kienhuis for providing technical support with the trace element analysis at
426 Utrecht University and Suzanne Verdegaal for supporting the measurements at the Vrije Universiteit
427 Amsterdam.

428

429 **References:**

430

431 Anand, P., Elderfield, H. and Conte, M.: Calibration of Mg/Ca thermometry in planktonic foraminifera from a
432 sediment trap time series, *Paleoceanography*, 18, 28–31, 2003.

433 Anand, P., Kroon, D., Singh, A., Ganeshram, R., Ganssen, G., and Elderfield, H.: Coupled sea surface
434 temperature–seawater $\delta^{18}\text{O}$ reconstructions in the Arabian Sea at the millennial scale for the last 35 ka,
435 *Paleoceanography*, 23, PA4207, doi: 10.1029/2007PA001564, 2008.

436 Backeberg, B. and Reason, C.: A connection between the South Equatorial Current north of Madagascar
437 and Mozambique Channel Eddies, *Geophys. Res. Lett.*, 37, L04604, doi: 10.1029/2009GL041950, 2010.

438 Barker, S., Greaves, M. and Elderfield, H.: A study of cleaning procedures used for foraminiferal Mg/Ca
439 paleothermometry, *Geochem. Geophys. Geosystems*, 4, 8407, 2003.

440 Bé, A. W.: Planktonic foraminifera, *Antarct. Map Folio Ser. Am. Geogr. Soc.*, 9–12, 1969.

441 Bé, A. W. H.: An ecological, zoogeographic and taxonomic review of recent planktonic foraminifera, *Ocean.*
442 *Micropalaeontology*, 1, 305-316, 1977.

443 Bé, A. W., Hemleben, C., Anderson, O. R. and Spindler, M.: Chamber formation in planktonic foraminifera,
444 *Micropaleontology*, 25, 294–307, 1979.

445 Bé, A. W. H.: Gametogenic calcification in a spinose planktonic foraminifer, *Globigerinoides sacculifer*
446 (Brady), *Mar. Micropaleontol.*, 5, 283–310, doi:10.1016/0377-8398(80)90014-6, 1980.

447 Bé, A. W. and Spero, H. J.: Shell regeneration and biological recovery of planktonic foraminifera after
448 physical injury induced in laboratory culture, *Micropaleontology*, 27, 305–316, 1981.

449 Bemis, B. E., Spero, H. J., Bijma, J. and Lea, D. W.: Reevaluation of the oxygen isotopic composition of
450 planktonic foraminifera: Experimental results and revised paleotemperature equations, *Paleoceanography*,
451 13(2), 150–160, doi:10.1029/98PA00070, 1998.

452 Berger, W., Killingley, J. and Vincent, E.: Sable isotopes in deep-sea carbonates-box core erdc-92, west
453 equatorial pacific, *Oceanol. Acta*, 1, 203–216, 1978.

454 Bijma, J., Spero, H. and Lea, D.: Reassessing foraminiferal stable isotope geochemistry: Impact of the
455 oceanic carbonate system (experimental results), in *Use of proxies in paleoceanography*, pp. 489–512,
456 Springer, Berlin Heidelberg, 1999.

457 Birch, H., Coxall, H. K., Pearson, P. N., Kroon, D. and O'Regan, M.: Planktonic foraminifera stable isotopes
458 and water column structure: Disentangling ecological signals, *Mar. Micropaleontol.*, 10, 127-145, 2013.

459 Brady, H.: Foraminifera in Tizard and Murray's Exploration of the Faroe Channel, vol. 11. In *Proc. Roy. Soc.*,
460 1882.

461 Brady, H.: Foraminifera in Tizard and Murray's Exploration of the Faroe Channel, vol. 11. 1882.

462 Brummer, G.-J. A., Hemleben, C. and Spindler, M.: Planktonic foraminiferal ontogeny and new perspectives
463 for micropalaeontology, *Nature*, 319(6048), 50–52, doi:10.1038/319050a0, 1986.

464 Brummer, G.-J. A., Hemleben, C. and Spindler, M.: Ontogeny of extant spinose planktonic foraminifera
465 (*Globigerinidae*): A concept exemplified by *Globigerinoides sacculifer* (Brady) and *G. ruber* (d'Orbigny), *Mar.*
466 *Micropaleontol.*, 12, 357–381, doi:10.1016/0377-8398(87)90028-4, 1987.

467 Cléroux, C., Cortijo, E., Duplessy, J. and Zahn, R.: Deep-dwelling foraminifera as thermocline temperature
468 recorders, *Geochem. Geophys. Geosystems*, 8, 2007.

469 Cléroux, C., Cortijo, E., Anand, P., Labeyrie, L., Bassinot, F., Caillon, N. and Duplessy, J.-C.: Mg/Ca and
470 Sr/Ca ratios in planktonic foraminifera: Proxies for upper water column temperature reconstruction,
471 *Paleoceanography*, 23, PA3214, doi: 10.1029/2007pa001505, 2008.

472 Cléroux, C., deMenocal, P., Arbuszewski, J. and Linsley, B.: Reconstructing the upper water column thermal
473 structure in the Atlantic Ocean, *Paleoceanography*, 28(3), 503–516, doi: 10.1002/palo.20050, 2013.

474 Curry, W. B. and Crowley, T. J.: The $\delta^{13}\text{C}$ of equatorial Atlantic surface waters: Implications for ice age pCO_2
475 levels, *Paleoceanography*, 2, 489–517, 1987.

476 Curry, W. B., Thunell, R. C. and Honjo, S.: Seasonal changes in the isotopic composition of planktonic
477 foraminifera collected in Panama Basin sediment traps, *Earth Planet. Sci. Lett.*, 64, 33–43, doi:
478 10.1016/0012-821X(83)90050-X, 1983.

479 Damassa, T. D., Cole, J. E., Barnett, H. R., Ault, T. R. and McClanahan, T. R.: Enhanced multidecadal
480 climate variability in the seventeenth century from coral isotope records in the western Indian Ocean,
481 *Paleoceanography*, 21, PA2016, doi: 10.1029/2005PA001217, 2006.

482 Deuser, W. G.: Variability of hydrography and particle flux: Transient and long-term relationships, *Mitt. Geol.-*
483 *Palaeont. Inst. Univ. Hambg.*, 62, 179–193, 1987.

484 Deuser, W. G. and Ross, E. H.: Seasonally abundant planktonic foraminifera of the Sargasso Sea;
485 succession, deep-water fluxes, isotopic compositions, and paleoceanographic implications, *J. Foraminifer.*
486 *Res.*, 19, 268–293, doi: 10.2113/gsjfr.19.4.268, 1989.

487 Deuser, W., Ross, E., Hemleben, C. and Spindler, M.: Seasonal changes in species composition, numbers,
488 mass, size, and isotopic composition of planktonic foraminifera settling into the deep Sargasso Sea,
489 *Palaeogeogr. Palaeoclimatol. Palaeoecol.*, 33, 103–127, 1981.

490 Duplessy, J. C., Bé, A. W. H. and Blanc, P. L.: Oxygen and carbon isotopic composition and biogeographic
491 distribution of planktonic foraminifera in the Indian Ocean, *Palaeogeogr. Palaeoclimatol. Palaeoecol.*, 33,
492 9–46, doi: 10.1016/0031-0182(81)90031-6, 1981.

493 Durgadoo, J.V., Loveday, B.R., Reason, C.J., Penven, P., Biastoch, A.: Agulhas leakage predominantly
494 responds to the Southern Hemisphere Westerlies. *J. Phys. Oceanogr.* 43, 2113–2131.
495 <http://dx.DOI.org/10.1175/JPO-D-13-047.1>, 2013

496 Eggins, S., De Deckker, P. and Marshall, J.: Mg/Ca variation in planktonic foraminifera tests: Implications
497 for reconstructing palaeo-seawater temperature and habitat migration, *Earth Planet. Sci. Lett.*, 212, 291–
498 306, 2003.

499 Eguchi, N. O., Ujiie, H., Kawahata, H. and Taira, A.: Seasonal variations in planktonic foraminifera at three
500 sediment traps in the subarctic, transition and subtropical zones of the central North Pacific Ocean, *Mar.*
501 *Micropaleontol.*, 48, 149–163, 2003.

502 Elderfield, H., Bertram, C. J. and Erez, J.: A biomineralization model for the incorporation of trace elements
503 into foraminiferal calcium carbonate, *Earth Planet. Sci. Lett.*, 142, 409–423, doi: 10.1016/0012-
504 821X(96)00105-7, 1996.

505 Elderfield, H. and Ganssen, G.: Past temperature and ^{18}O of surface ocean waters inferred from
506 foraminiferal Mg/Ca ratios, *Nature*, 405, 442–445, 2000.

507 Emiliani, C.: Depth habitats of some species of pelagic Foraminifera as indicated by oxygen isotope ratios,
508 *Am. J. Sci.*, 252, 149–158, doi: 10.2475/ajs.252.3.149, 1954.

509 Epstein, S. and Mayeda, T.: Variation of O^{18} content of waters from natural sources, *Geochim. Cosmochim.*
510 *Acta*, 4, 213–224, 1953.

511 Erez, J.: Vital effect on stable-isotope composition seen in foraminifera and coral skeletons, *Nature* 273,
512 199-202, doi:10.1038/273199a0, 1978.

513 Erez, J.: The source of ions for biomineralization in foraminifera and their implications for paleoceanographic
514 proxies, *Rev. Mineral. Geochem.*, 54, 115–149, 2003.

515 Erez, J. and Honjo, S.: Comparison of isotopic composition of planktonic foraminifera in plankton tows,
516 sediment traps and sediments, *Palaeogeogr. Palaeoclimatol. Palaeoecol.*, 33, 129–156, doi:10.1016/0031-
517 0182(81)90035-3, 1981.

518 Fairbanks, R. G., Wiebe, P. H. and Bé, A. W.: Vertical distribution and isotopic composition of living
519 planktonic foraminifera in the western North Atlantic, *Science*, 207, 61–63, 1980.

520 Fairbanks, R. G., Sverdrlove, M., Free, R., Wiebe, P. H. and Bé, A. W.: Vertical distribution and isotopic
521 fractionation of living planktonic foraminifera from the Panama Basin, *Nature*, 298, 841–844, 1982.

522 Falkowski, P. G., Ziemann, D., Kolber, Z. and Bienfang, P. K.: Role of eddy pumping in enhancing primary
523 production in the ocean, *Nature* 352, 55-58, doi:10.1038/352055a0, 1991.

524 Fallet, U., Boer, W., van Assen, C., Greaves, M. and Brummer, G.-J. A.: A novel application of wet oxidation
525 to retrieve carbonates from large organic-rich samples for ocean-climate research, *Geochem Geophys*
526 *Geosyst*, 10, Q08004, doi: 10.1029/2009gc002573, 2009.

527 Fallet, U., Brummer, G.-J., Zinke, J., Vogels, S. and Ridderinkhof, H.: Contrasting seasonal fluxes of
528 planktonic foraminifera and impacts on paleothermometry in the Mozambique Channel upstream of the
529 Agulhas Current, *Paleoceanography*, 25, PA4223, doi: 10.1029/2010pa001942, 2010.

530 Fallet, U., Ullgren, J. E., Castañeda, I. S., van Aken, H. M., Schouten, S., Ridderinkhof, H. and Brummer,
531 G.-J. A.: Contrasting variability in foraminiferal and organic paleotemperature proxies in sedimenting
532 particles of the Mozambique Channel (SW Indian Ocean), *Geochim. Cosmochim. Acta*, 75, 5834–5848,
533 2011.

534 Fallet, U., Castañeda, I. S., Henry-Edwards, A., Richter, T. O., Boer, W., Schouten, S. and Brummer, G.-J.:
535 Sedimentation and burial of organic and inorganic temperature proxies in the Mozambique Channel, SW
536 Indian Ocean, *Deep Sea Res. Part Oceanogr. Res. Pap.*, 59, 37–53, 2012.

537 Farmer, E. C., Kaplan, A., de Menocal, P. B. and Lynch-Stieglitz, J.: Corroborating ecological depth
538 preferences of planktonic foraminifera in the tropical Atlantic with the stable oxygen isotope ratios of core
539 top specimens, *Paleoceanography*, 22(3), doi:DOI: 10.1029/2006PA001361, 2007.

540 Faul, K. L., Ravelo, A. C. and Delaney, M. L.: Reconstructions of Upwelling, Productivity, and Photic Zone
541 Depth in the Eastern Equatorial Pacific Ocean Using Planktonic Foraminiferal Stable Isotopes and
542 Abundances, *J. Foraminifer. Res.*, 30, 110–125, doi: 10.2113/0300110, 2000.

543 Field, D. B.: Variability in vertical distributions of planktonic foraminifera in the California Current:
544 Relationships to Vertical Ocean structure, *Paleoceanography*, 19, PA2014, doi:10.1029/2003PA000970,
545 2004.

546 Friedrich, O., Schiebel, R., Wilson, P. A., Weldeab, S., Beer, C. J., Cooper, M. J. and Fiebig, J.: Influence
547 of test size, water depth, and ecology on Mg/Ca, Sr/Ca, $\delta^{18}\text{O}$ and $\delta^{13}\text{C}$ in nine modern species of planktic
548 foraminifers, *Earth Planet. Sci. Lett.*, 319, 133–145, doi: 10.1016/j.epsl.2011.12.002, 2012.

549 Ganssen, G. and Sarnthein, M.: Stable-Isotope Composition of Foraminifers: The Surface and Bottom Water
550 Record of Coastal Upwelling, in *Coastal Upwelling Its Sediment Record*, edited by E. Suess and J. Thiede,
551 pp. 99–121, Springer US. [online] Available from: http://link.springer.com/chapter/10.1007/978-1-4615-6651-9_6 (Accessed 5 December 2013), 1983.

553 Grossman, E. L.: Stable isotopes in modern benthic foraminifera; a study of vital effect, *J. Foraminifer. Res.*,
554 17, 48–61, 1987.

555 Gründlingh, M. L.: Tracking eddies in the southeast Atlantic and southwest Indian oceans with
556 TOPEX/POSEIDON, *J. Geophys. Res.*, 100, 24977–24,986, 1995.

557 Hastenrath, S., Nicklis, A. and Greischar, L.: Atmospheric-hydrospheric mechanisms of climate anomalies
558 in the western equatorial Indian Ocean, *J. Geophys. Res. Oceans*, 98, 20219–20235, doi:
559 10.1029/93JC02330, 1993.

560 Hathorne, E. C., James, R. H. and Lampitt, R. S.: Environmental versus biomineralization controls on the
561 intratest variation in the trace element composition of the planktonic foraminifera *G. inflata* and *G. scitula*,
562 *Paleoceanography*, 24, PA4204, doi: 10.1029/2009pa001742, 2009.

563 Hemleben, C. and Bijma, J.: Foraminiferal population dynamics and stable carbon isotopes, in *Carbon*
564 *Cycling in the Glacial Ocean: Constraints on the Ocean's Role in Global Change*, Springer, Berlin
565 Heidelberg, 145–166, 1994.

566 Hemleben, C., Spindler, M. and Anderson, O.: *Modern planktonic foraminifera*, Springer, Berlin, 363 pp.,
567 1989.

568 Huang, K., You, C., Lin, H. and Shieh, Y.: In situ calibration of Mg/Ca ratio in planktonic foraminiferal shell
569 using time series sediment trap: A case study of intense dissolution artifact in the South China Sea,
570 *Geochem. Geophys. Geosystems*, 9, Q04016, doi:10.1029/207GC001660, 2008.

571 Hut, G.: *Stable Isotope Reference Samples for Geochemical and Hydrological Investigations*. Rep. to Dir.
572 Gen., International Atomic Energy Agency, Vienna, 42 pp., 1987.

573 Itou, M., Ono, T., Oba, T. and Noriki, S.: Isotopic composition and morphology of living *Globorotalia scitula*:
574 a new proxy of sub-intermediate ocean carbonate chemistry?, *Mar. Micropaleontol.*, 42, 189–210, 2001.

575 Jonkers, L., de Nooijer, L., Reichart, G., Zahn, R. and Brummer, G.: Encrustation and trace element
576 composition of *Neogloboquadrina dutertrei* assessed from single chamber analyses, implications for
577 paleotemperature estimates, *Biogeosciences*, 9, 4851–4860, doi:10.5194/bg-9-4851-2012, 2012.

578 Kahn, M. I.: Non-equilibrium oxygen and carbon isotopic fractionation in tests of living planktic foraminifera
579 from the eastern equatorial Atlantic Ocean, Ph.D. thesis, University of South California, Los Angeles, 224
580 p., 1977.

581 Kahn, M.: Non-equilibrium oxygen and carbon isotopic fractionation in tests of living planktonic-foraminifera,
582 *Oceanol. Acta*, 2, 195–208, 1979.

583 Kahn, M. I. and Williams, D. F.: Oxygen and carbon isotopic composition of living planktonic foraminifera
584 from the northeast Pacific Ocean, *Palaeogeogr. Palaeoclimatol. Palaeoecol.*, 33, 47–69, 1981.

585 Kiefer, T., McCave, I. N. and Elderfield, H.: Antarctic control on tropical Indian Ocean sea surface
586 temperature and hydrography, *Geophys. Res. Lett.*, 33, L24612, doi:10.1029/2006GL027097, 2006.

587 Kim, S.-T. and O'Neil, J. R.: Equilibrium and nonequilibrium oxygen isotope effects in synthetic carbonates,
588 *Geochim. Cosmochim. Acta*, 61, 3461–3475, doi: 10.1016/S0016-7037(97)00169-5, 1997.

589 Kolasinski, J., Kaehler, S. and Jaquemet, S.: Distribution and sources of particulate organic matter in a
590 mesoscale eddy dipole in the Mozambique Channel (south-western Indian Ocean): Insight from C and N
591 stable isotopes, *J. Mar. Syst.*, 96-97, 122-131, doi:10.1016/j.jmarsys.2012.02.015, 2012.

592 Kroon, D. and Darling, K.: Size and upwelling control of the stable isotope composition of *Neogloboquadrina*
593 *dutertrei* (d'Orbigny), *Globigerinoides ruber* (d'Orbigny) and *Globigerina bulloides* d'Orbigny; examples from
594 the Panama Basin and Arabian Sea, *J. Foraminifer. Res.*, 25, 39–52, 1995.

595 Kunioka, D., Shirai, K., Takahata, N., Sano, Y., Toyofuku, T. and Ujiie, Y.: Microdistribution of Mg/Ca, Sr/Ca,
596 and Ba/Ca ratios in *Pulleniatina obliquiloculata* test by using a NanoSIMS: Implication for the vital effect
597 mechanism, *Geochem. Geophys. Geosystems*, 7, Q12P20, doi:10.1029/2006GC001280, 2006.

598 Kuroyanagi, A. and Kawahata, H.: Vertical distribution of living planktonic foraminifera in the seas around
599 Japan, *Mar. Micropaleontol.*, 53, 173–196, doi: 10.1016/j.marmicro.2004.06.001, 2004.

600 Lévy, M.: Mesoscale variability of phytoplankton and of new production: Impact of the large-scale nutrient
601 distribution, *J. Geophys. Res. Oceans* 1978–2012, 108, 3358, doi:10.1029/2002JC001577, 2003.

602 Lin, H.-L. and Hsieh, H.-Y.: Seasonal variations of modern planktonic foraminifera in the South China Sea,
603 *Deep Sea Res. Part II Top. Stud. Oceanogr.*, 54, 1634–1644, 2007.

604 Lohmann, G. P.: A model for variation in the chemistry of planktonic foraminifera due to secondary
605 calcification and selective dissolution, *Paleoceanography*, 10(3), 445–457, doi:10.1029/95PA00059, 1995.

606 Lončarić, N., van Iperen, J., Kroon, D. and Brummer, G.-J. A.: Seasonal export and sediment preservation
607 of diatomaceous, foraminiferal and organic matter mass fluxes in a trophic gradient across the SE Atlantic,
608 *Prog. Oceanogr.*, 73, 27–59, 2007.

609 Lončarić, N., Peeters, F. J. C., Kroon, D. and Brummer, G. J. A.: Oxygen isotope ecology of recent planktic
610 foraminifera at the central Walvis Ridge (SE Atlantic), *Paleoceanography*, 21, 3009, 2006.

611 McClanahan, T. R.: Seasonality in East Africa's coastal waters., *Mar. Ecol. Prog. Ser. Oldendorf*, 44, 191–
612 199, 1988.

613 McCorkle, D. C., Keigwin, L. D., Corliss, B. H. and Emerson, S. R.: The influence of microhabitats on the
614 carbon isotopic composition of deep-sea benthic foraminifera, *Paleoceanography*, 5, 161–185, 1990.

615 Mohtadi, M., Hebbeln, D., Nuñez Ricardo, S. and Lange, C. B.: El Niño-like pattern in the Pacific during
616 marine isotope stages (MIS) 13 and 11?, *Paleoceanography*, 21, PA1015, doi:10.1029/2005PA001190,
617 2006.

618 Mulitza, S., Dürkoop, A., Hale, W., Wefer, G. and Niebler, H. S.: Planktonic foraminifera as recorders of past
619 surface-water stratification, *Geology*, 25, 335–338, doi: 10.1130/0091-7613, 1997.

620 Mulitza, S., Arz, H., Kemle-von Mücke, S., Moos, C., Niebler, H.-S., Pätzold, J. and Segl, M.: The South
621 Atlantic carbon isotope record of planktic foraminifera, in *Use of Proxies in Paleoceanography*, pp. 427–
622 445, Springer., 1999.

623 New, A., Alderson, S., Smeed, D. and Stansfield, K.: On the circulation of water masses across the
624 Mascarene Plateau in the South Indian Ocean, *Deep Sea Res. Part Oceanogr. Res. Pap.*, 54, 42–74, 2007.

625 Oppo, D. W. and Fairbanks, R. G.: Carbon isotope composition of tropical surface water during the past
626 22,000 years, *Paleoceanography*, 4, 333–351, 1989.

627 D'Orbigny, A.: Foraminifères, *Hist. Phys. Polit. Nat. Lî Cuba Bertrand Paris*, 1839.

628 Ortiz, J., Mix, A., Rugh, W., Watkins, J. and Collier, R.: Deep-dwelling planktonic foraminifera of the
629 northeastern Pacific Ocean reveal environmental control of oxygen and carbon isotopic disequilibria,
630 *Geochim. Cosmochim. Acta*, 60, 4509–4523, 1996.

631 Patrick, A. and Thunell, R. C.: Tropical Pacific sea surface temperatures and upper water column thermal
632 structure during the last glacial maximum, *Paleoceanography*, 12, 649–657, 1997.

633 Parker, W. K., Jones, T. R., Bailey, J. and Pourtales, F.: On some foraminifera from the north Atlantic and
634 Arctic Oceans, including Davis Straits and Baffin's Bay, *Philos. Trans. R. Soc. Lond.*, 155, 325–441, 1865.

635 Peeters, F. J. C. and Brummer, G.-J. A.: The seasonal and vertical distribution of living planktic foraminifera
636 in the NW Arabian Sea, *Geol. Soc. Lond. Spec. Publ.*, 195, 463–497, doi: 10.1144/GSL.SP.2002.195.01.26,
637 2002

638 Peeters, F., Brummer, G. and Ganssen, G.: The effect of upwelling on the distribution and stable isotope
639 composition of *Globigerina bulloides* and *Globigerinoides ruber* (planktic foraminifera) in modern surface
640 waters of the NW Arabian Sea, *Glob. Planet. Change*, 34, 269–291, 2002.

641 Ravelo, A. and Fairbanks, R.: Oxygen isotopic composition of multiple species of planktonic foraminifera:
642 Records of the modern photic zone temperature gradient, *Paleoceanography*, 7, 815–831, 1992.

643 Ravelo, A. and Fairbanks, R.: Carbon isotopic fractionation in multiple species of planktonic foraminifera
644 from core-tops in the tropical Atlantic, *J. Foraminiferal Res.* 25, 53–74, doi:10.2113/gsjfr.25.1.53, 1995.

645 Ravelo, A., Fairbanks, R. and Philander, S.: Reconstructing tropical Atlantic hydrography using planktonic
646 foraminifera and an ocean model, *Paleoceanography*, 5, 409–431, 1990.

647 Regenberg, M., Steph, S., Nürnberg, D., Tiedemann, R. and Garbe-Schönberg, D.: Calibrating Mg/Ca ratios
648 of multiple planktonic foraminiferal species with $\delta^{18}\text{O}$ -calcification temperatures: Paleothermometry for the
649 upper water column, *Earth Planet. Sci. Lett.*, 278(3–4), 324–336, doi:10.1016/j.epsl.2008.12.019, 2009.

650 Reichart, G.-J., Jorissen, F., Anschutz, P. and Mason, P. R.: Single foraminiferal test chemistry records the
651 marine environment, *Geology*, 31(4), 355–358, 2003.

652 Russell, A. D. and Spero, H. J.: Field examination of the oceanic carbonate ion effect on stable isotopes in
653 planktonic foraminifera, *Paleoceanography*, 15(1), 43–52, 2000.

654 Sadekov, A., Eggins, S. M., De Deckker, P., Ninnemann, U., Kuhnt, W. and Bassinot, F.: Surface and
655 subsurface seawater temperature reconstruction using Mg/Ca microanalysis of planktonic foraminifera
656 *Globigerinoides ruber*, *Globigerinoides sacculifer*, and *Pulleniatina obliquiloculata*, *Paleoceanography*, 24,
657 PA3201, doi:10.1029/2008PA001664, 2009.

658 Schmidt, G.A., G. R. Bigg and E. J. Rohling. 1999. "Global Seawater Oxygen-18 Database - v1.21"
659 <http://data.giss.nasa.gov/o18data/> (last access: 2 November 2014), 1999.

660 Shackleton, N.: Attainment of isotopic equilibrium between ocean water and the benthonic foraminifera
661 genus *Uvigerina*: isotopic changes in the ocean during the last glacial, *Les methods quantitatives d'etude*

662 des variations du climat au cours du Pleistocene, Gif-sur-Yvette, Colloque international du CNRS, 219, 203–
663 210, 1974.

664 Spero, H. J. and Lea, D. W.: Intraspecific stable isotope variability in the planktic foraminifera
665 *Globigerinoides sacculifer*: Results from laboratory experiments, Mar. Micropaleontol., 22, 221–234, 1993.

666 Spero, H. J., Lerche, I. and Williams, D. F.: Opening the carbon isotope “vital effect” black box, 2,
667 Quantitative model for interpreting foraminiferal carbon isotope data, Paleoceanography, 6, 639–655, 1991.

668 Spero, H. J., Bijma, J., Lea, D. W. and Bemis, B. E.: Effect of seawater carbonate concentration on
669 foraminiferal carbon and oxygen isotopes, Nature, 390, 497–500, doi: 10.1038/37333, 1997.

670 Spero, H. J., Mielke, K. M., Kalve, E. M., Lea, D. W. and Pak, D. K.: Multispecies approach to reconstructing
671 eastern equatorial Pacific thermocline hydrography during the past 360 kyr, Paleoceanography, 18, 1022,
672 doi: 10.1029/2002PA000814, 2003.

673 Steinhardt, J., Cléroux, C., Ullgren, J., de Nooijer, L., Durgadoo, J. V., Brummer, G.-J. and Reichert, G.-J.:
674 Anti-cyclonic eddy imprint on calcite geochemistry of several planktonic foraminiferal species in the
675 Mozambique Channel, Mar. Micropaleontol., 113, 20–33, doi: 10.1016/j.marmicro.2014.09.001, 2014.

676 Steinke, S., Chiu, H., Yu, P., Shen, C., Löwemark, L., Mii, H. and Chen, M.: Mg/Ca ratios of two
677 *Globigerinoides ruber* (white) morphotypes: Implications for reconstructing past tropical/subtropical surface
678 water conditions, Geochem. Geophys. Geosystems, 6, Q11005, 2005.

679 Steph, S., Regenberg, M., Tiedemann, R., Mulitza, S. and Nürnberg, D.: Stable isotopes of planktonic
680 foraminifera from tropical Atlantic/Caribbean core-tops: Implications for reconstructing upper ocean
681 stratification, Mar. Micropaleontol., 71, 1–19, doi: 10.1016/j.marmicro.2008.12.004, 2009.

682 Swallow, J., Fieux, M. and Schott, F.: The boundary currents east and north of Madagascar: 1. Geostrophic
683 currents and transports, J. Geophys. Res. Oceans, 93, 4951–4962, 1988.

684 Tedesco, K., Thunell, R., Astor, Y. and Muller-Karger, F.: The oxygen isotope composition of planktonic
685 foraminifera from the Cariaco Basin, Venezuela: Seasonal and interannual variations, Mar. Micropaleontol.,
686 62, 180–193, doi:10.1016/j.marmicro.2006.08.002, 2007.

687 Tolderlund, D. S. and Bé, A. W.: Seasonal distribution of planktonic foraminifera in the western North
688 Atlantic, Micropaleontology, 17, 297–329, 1971.

689 Ullgren, J., van Aken, H., Ridderinkhof, H. and de Ruijter, W.: The hydrography of the Mozambique Channel
690 from six years of continuous temperature, salinity, and velocity observations, Deep-Sea Res., 69, 36–50,
691 2012.

692 Urey, H. C.: The thermodynamic properties of isotopic substances, J. Chem. Soc. (1926–1965), 562–581,
693 doi:10.1039/JR9470000562, 1947.

694 Vergnaud Grazzini, C.: Non-equilibrium isotopic compositions of shells of planktonic foraminifera in the
695 Mediterranean Sea, Palaeogeogr. Palaeoclimatol. Palaeoecol., 20, 263–276, 1976.

696 Vincent, E. and Berger, W.: Planktonic foraminifera and their use in paleoceanography, The sea, 7, 1025–
697 1119, 1981.

698 Watkins, J. M., Mix, A. C. and Wilson, J.: Living planktic foraminifera: tracers of circulation and productivity
699 regimes in the central equatorial Pacific, Deep Sea Res. Part II Top. Stud. Oceanogr., 43, 1257–1282, 1996.

700 Weibull, W.: A statistical theory of the strength of materials, Ingeniorsvetenskaps Akademiens Handlingar
701 NR. 151, 1939.

702 Wefer, G. and Berger, W. H.: Isotope paleontology: growth and composition of extant calcareous species,
703 Mar. Geol., 100, 207–248, 1991.

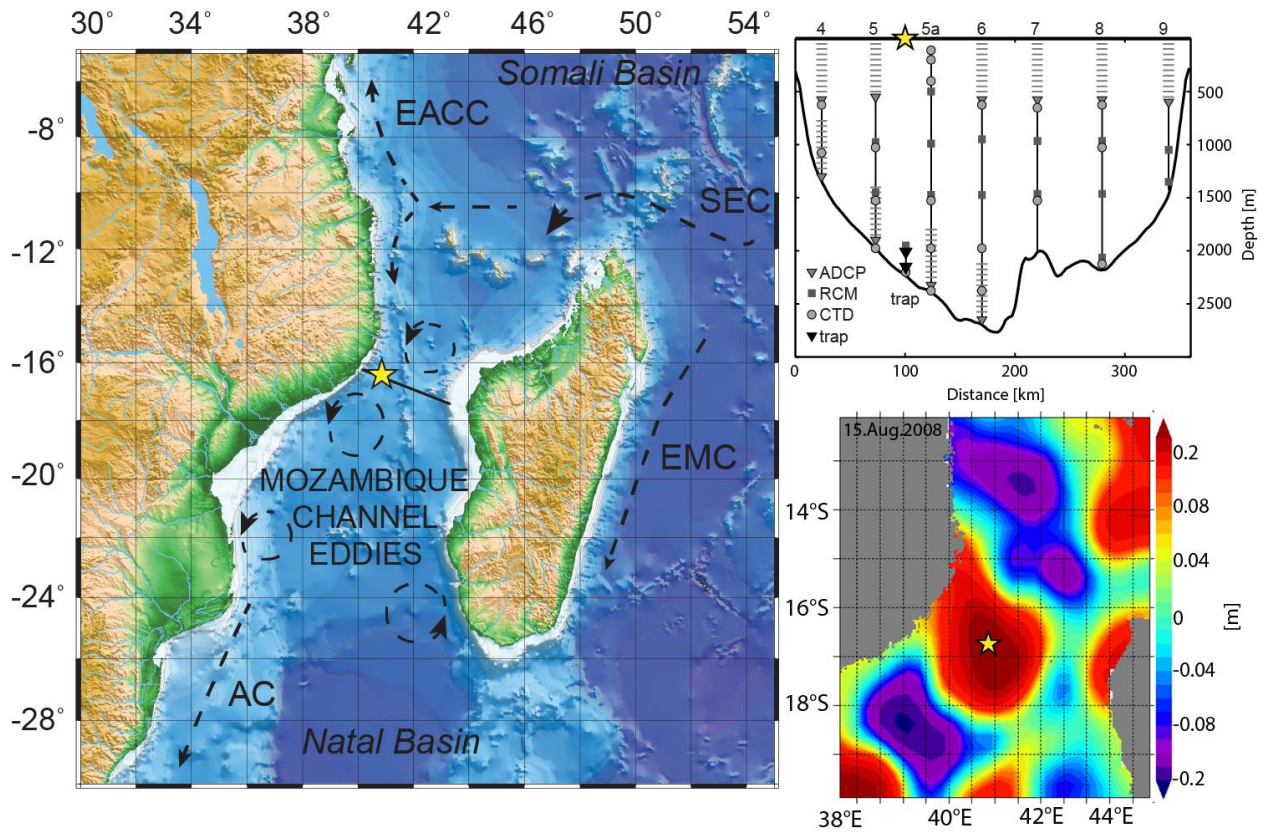
704 Wilke, I., Bickert, T. and Peeters, F. J.: The influence of seawater carbonate ion concentration [CO₃²⁻] on
705 the stable carbon isotope composition of the planktic foraminifera species *Globorotalia inflata*, Mar.
706 Micropaleontol., 58, 243–258, 2006.

707 Wilke, I., Meggers, H. and Bickert, T.: Depth habitats and seasonal distributions of recent planktic
708 foraminifers in the Canary Islands region (29°N) based on oxygen isotopes, Deep Sea Res., 56, 89–106,
709 doi: 10.1016/j.dsr.2008.08.001, 2009.

710 Wyrтки, K.: Physical oceanography of the Indian Ocean, in The biology of the Indian Ocean, Springer, Berlin
711 Heidelberg, 18–36, 1973.

712

713 **Figures:**



714

715 *Fig. 1*

716

species	Mg/Ca [mmol/mol]	Mg/Ca SD [mmol/mol]	Mg/Ca-based temperatures [°C]	$\delta^{18}\text{O}$ [‰]	$\delta^{18}\text{O}$ SD [‰]	$\delta^{18}\text{O}$ -based temperatures [°C]	$\delta^{13}\text{C} \pm \text{SE}$ [‰]	$\delta^{13}\text{C}$ SD [‰]
<i>G. ruber</i>	5.3±0.09	±1.2	28.1±2.8	-2.57±0.04	±0.35	29.4±1.3	0.51±0.03	±0.47
<i>N. dutertrei</i>	2.6±0.06	±1.0	22.5±3.7	-1.53±0.03	±0.48	24.3±2.0	0.53±0.04	±0.44
<i>P. obliquiloculata</i>	2.3±0.1	±0.6	21.6±3.1	-1.13±0.04	±0.24	22.3±1.1	0.04±0.04	±0.21
<i>G. scitula</i>	1.5±0.07	±0.4	14.4±3.4	1.47±0.14	±0.87	14.4±3.9*	0.27±0.04	±0.22

* vital effect corrected [Kahn an Williams, 1981]

data from Steinhardt et al. 2014

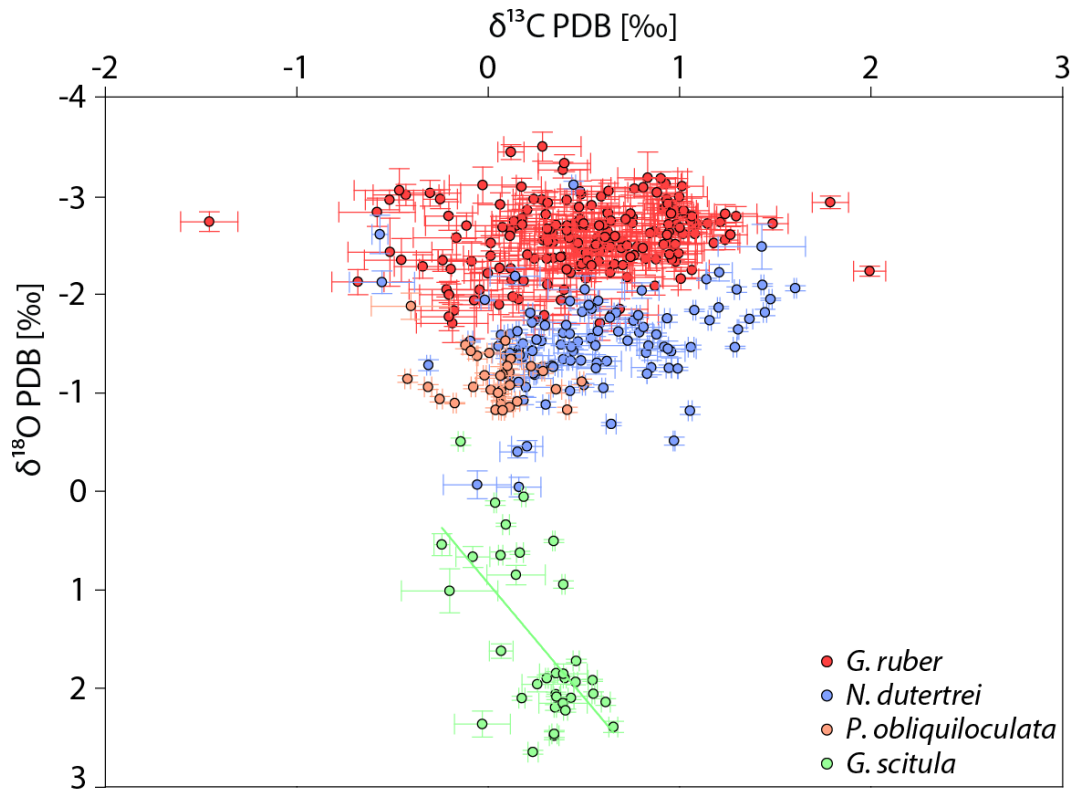
717 **Tab. 1**

718

species	$\delta^{13}\text{C}$ [‰]		$\delta^{13}\text{C}$ SD [‰]		$\delta^{18}\text{O}$ [‰]		$\delta^{18}\text{O}$ SD [‰]	
	VU	BCN	VU	BCN	VU	BCN	VU	BCN
<i>G. rub</i>	-	0.51±0.03	-	±0.47	-	-2.57±0.04	-	0.35
<i>N. dut</i>	0.41±0.12	0.54±0.01	0.41	0.45	-1.37±0.09	-1.58±0.03	0.59	0.46
<i>P. obli</i>	-0.07±0.13	0.05±0.01	0.29	0.20	-1.46±0.09	-1.10±0.02	0.37	0.21
<i>G. scit</i>	0.13±0.14	0.3±0.02	0.24	0.21	1.55±0.11	1.45±0.04	0.69	0.92

719 **Tab. 2**

720



721

722 Fig. 2

Species	$\delta^{18}\text{O} \pm \text{SE}$ [‰]		$\delta^{18}\text{O}$ SD [‰]		T [°C], (Kim&O'Neil, 1997)		$\delta^{13}\text{C} \pm \text{SE}$ [‰]		$\delta^{13}\text{C}$ SD [‰]	
	Eddy	Non-Eddy	Eddy	Non-Eddy	Eddy	Non-Eddy	Eddy	Non-Eddy	Eddy	Non-Eddy
<i>G. ruber</i>	-2.56±0.03	-2.57±0.04	0.31	0.39	29.8	29.2	0.59±0.04	0.39±0.06	0.40	0.53
<i>N. dutertrei</i>	-1.53±0.08	-1.53±0.05	0.58	0.39	24.6	24.0	0.39±0.06	0.64±0.04	0.44	0.41
<i>P. obliquiloculata</i>	-1.25±0.06	-1.09±0.05	0.19	0.25	23.3	21.9	0.18±0.06	-0.02±0.04	0.18	0.19
<i>G. scitula</i>	1.99±0.1	1.18±0.2	0.48	0.92	8.2	11.5	0.31±0.05	0.25±0.06	0.18	0.26

723 *Tab. 3*

724

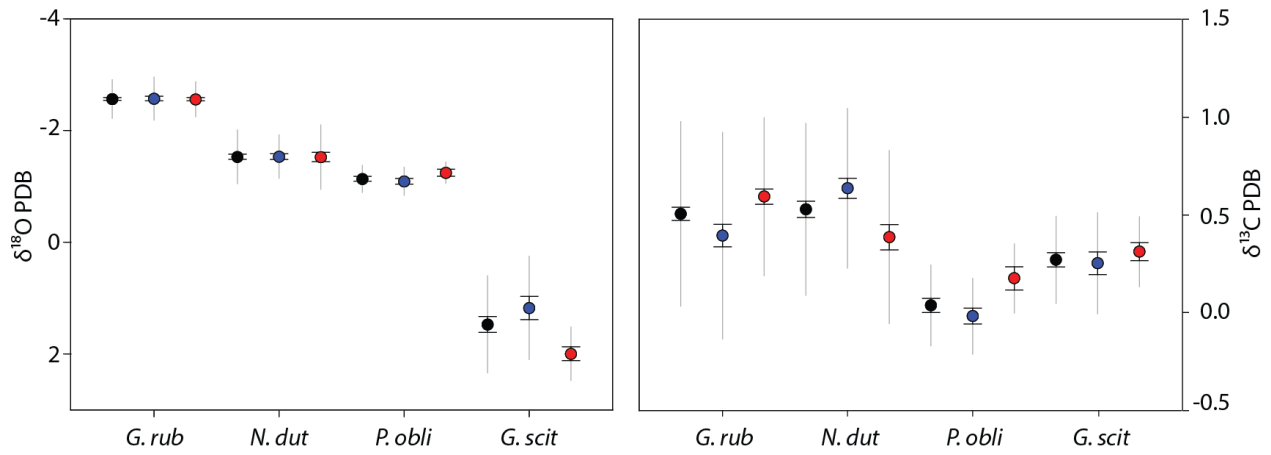


Figure 3

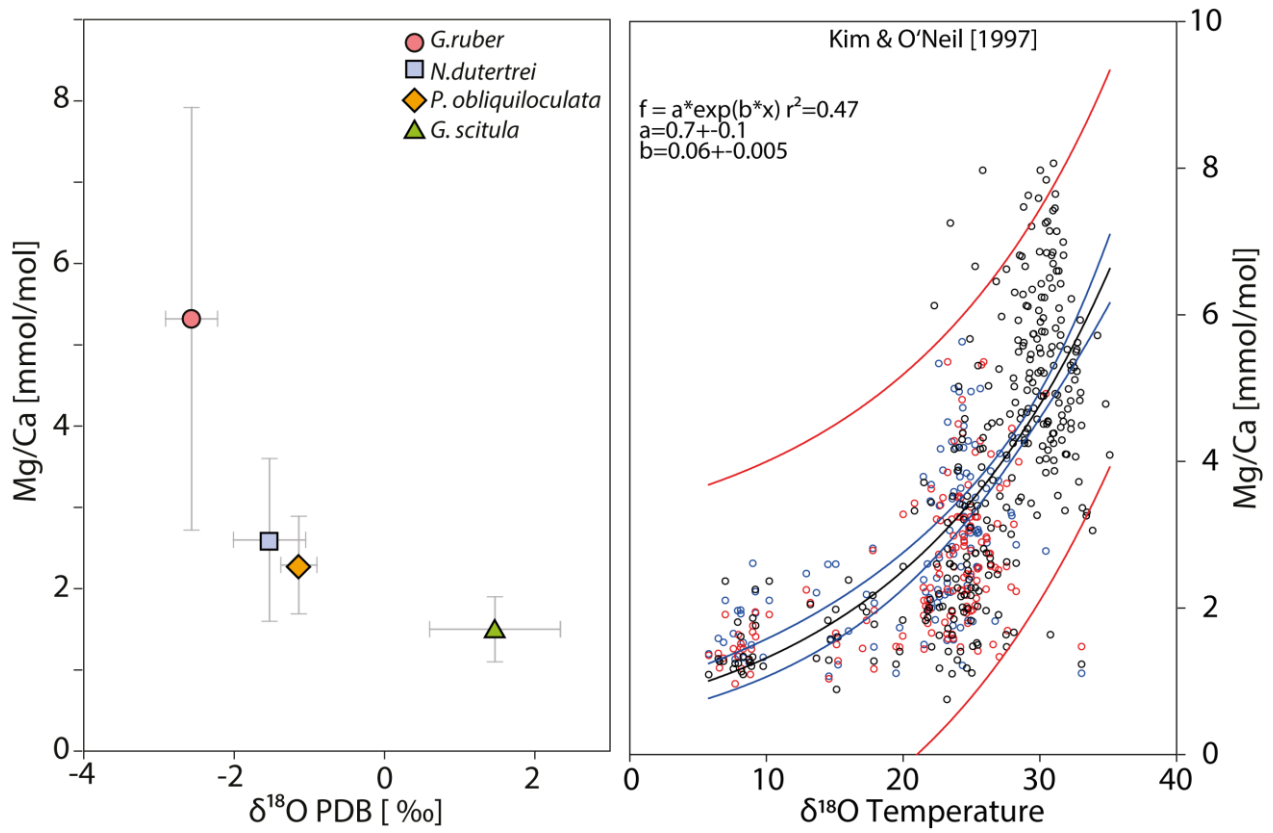


Figure 4

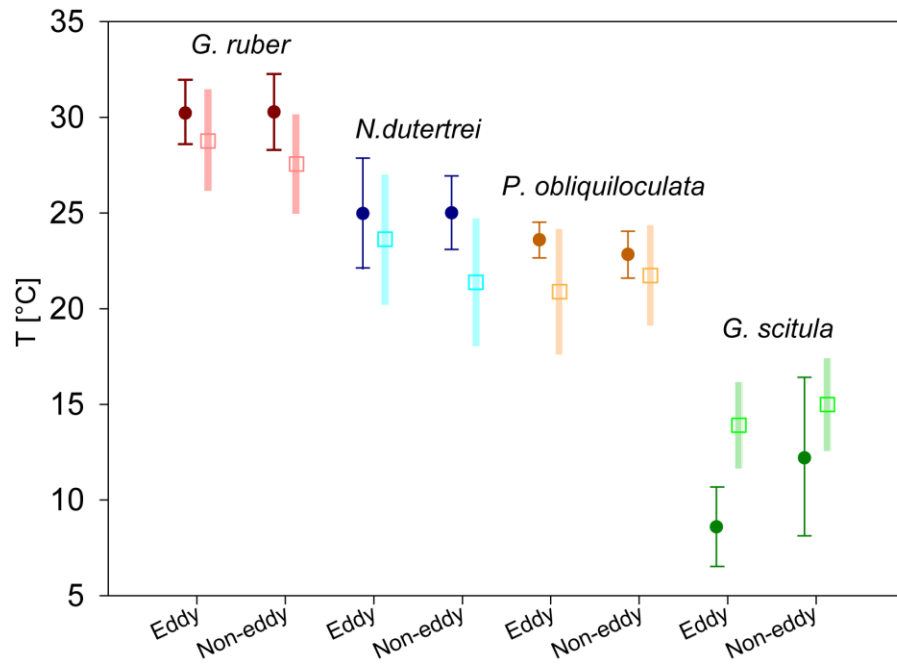


Figure 5

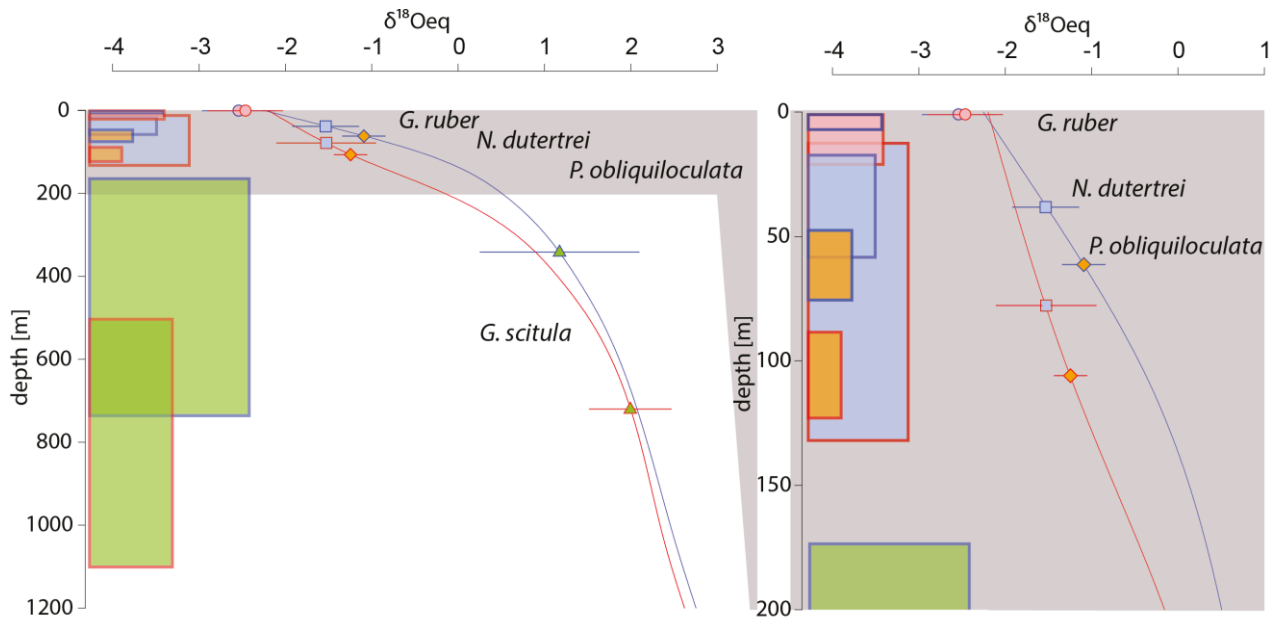
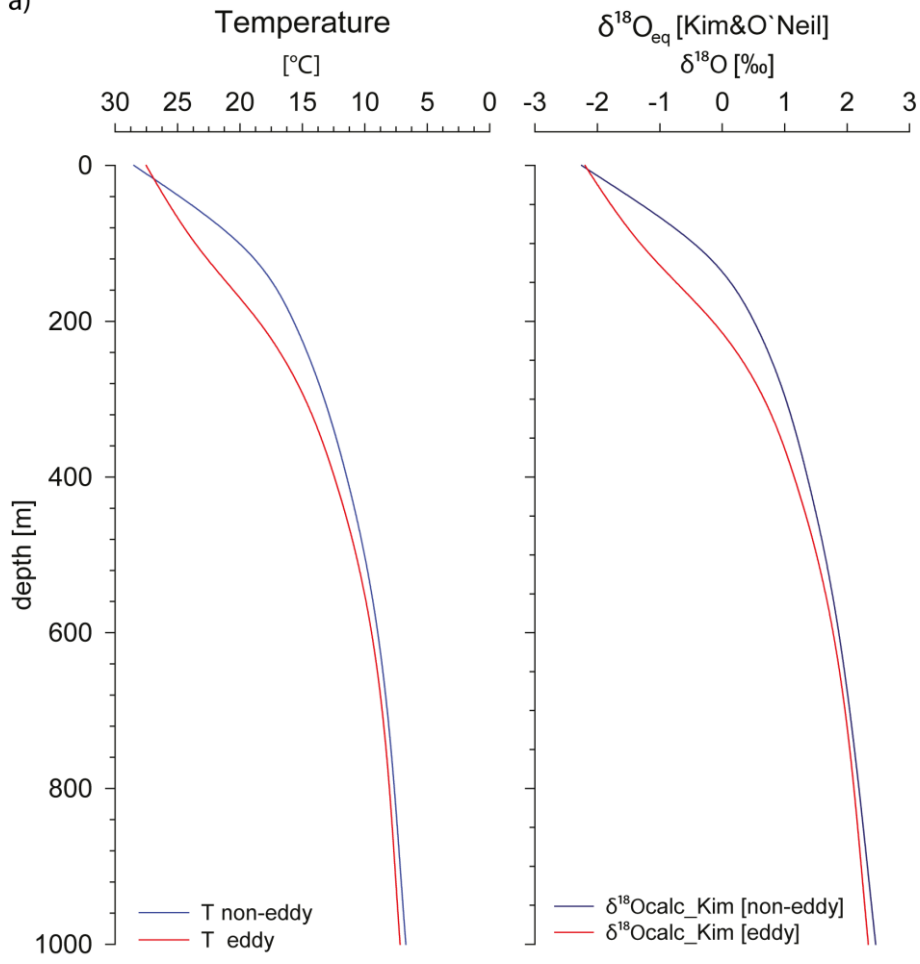


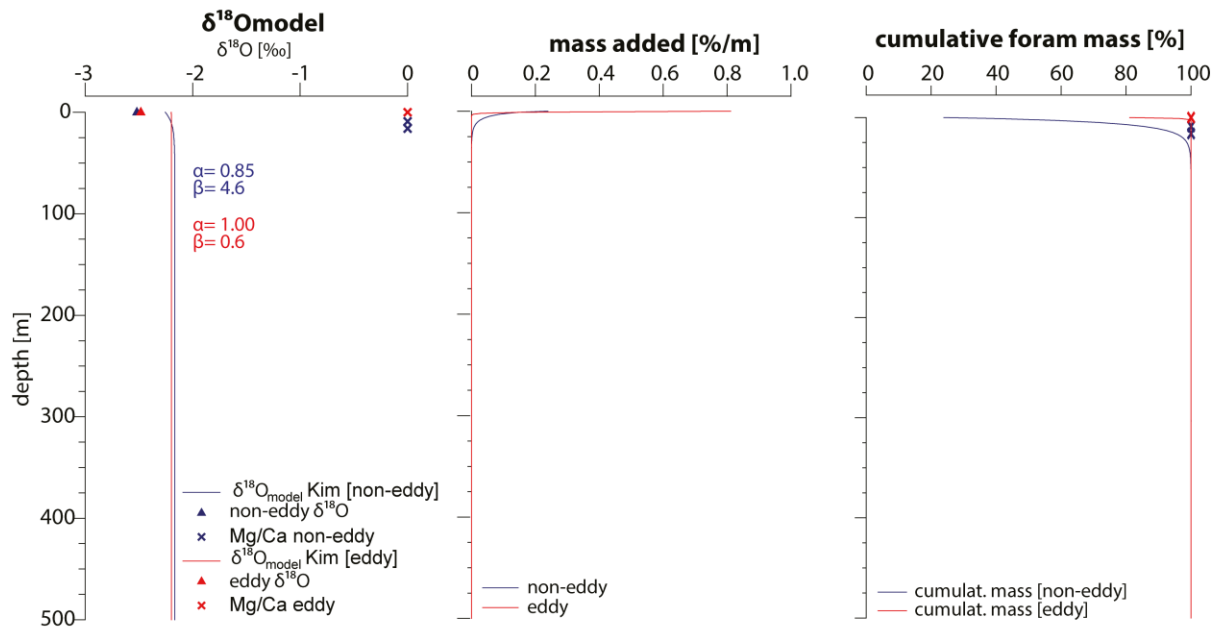
Figure 6

a)



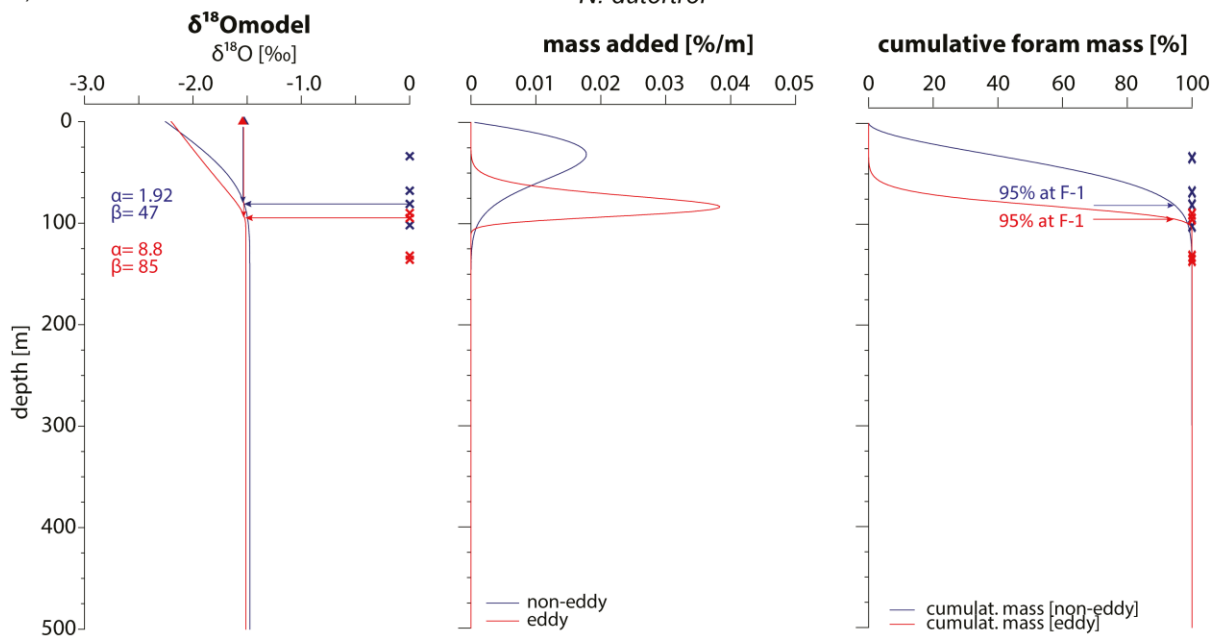
b)

G. ruber



c)

N. dutertrei



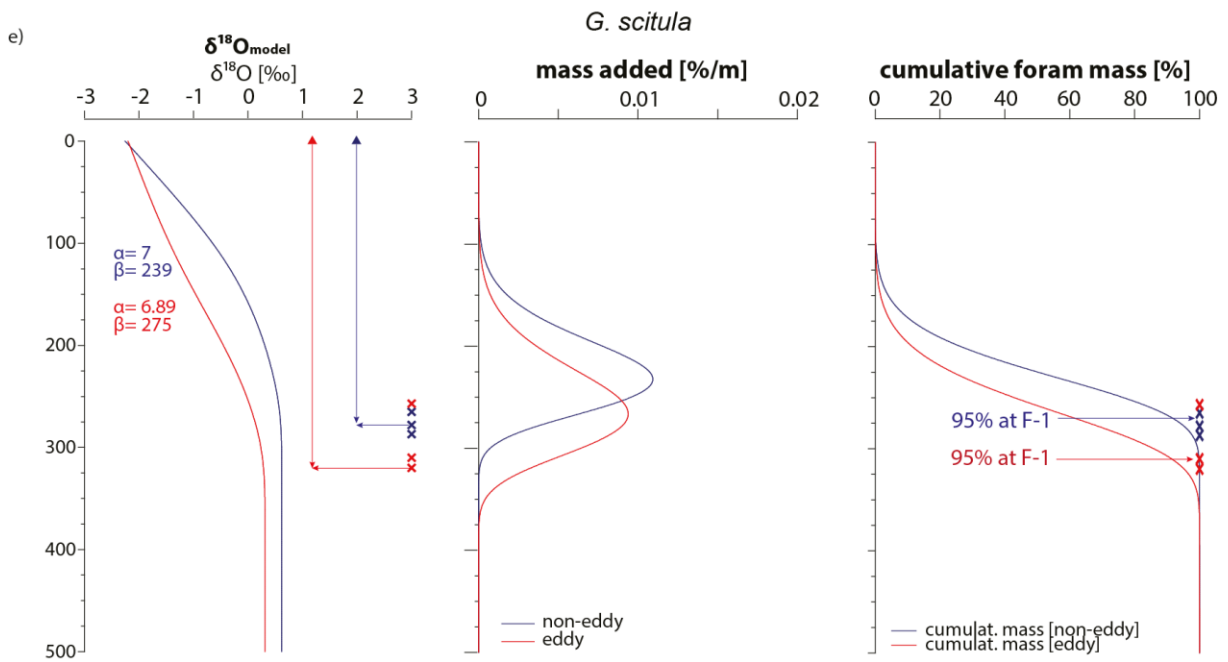
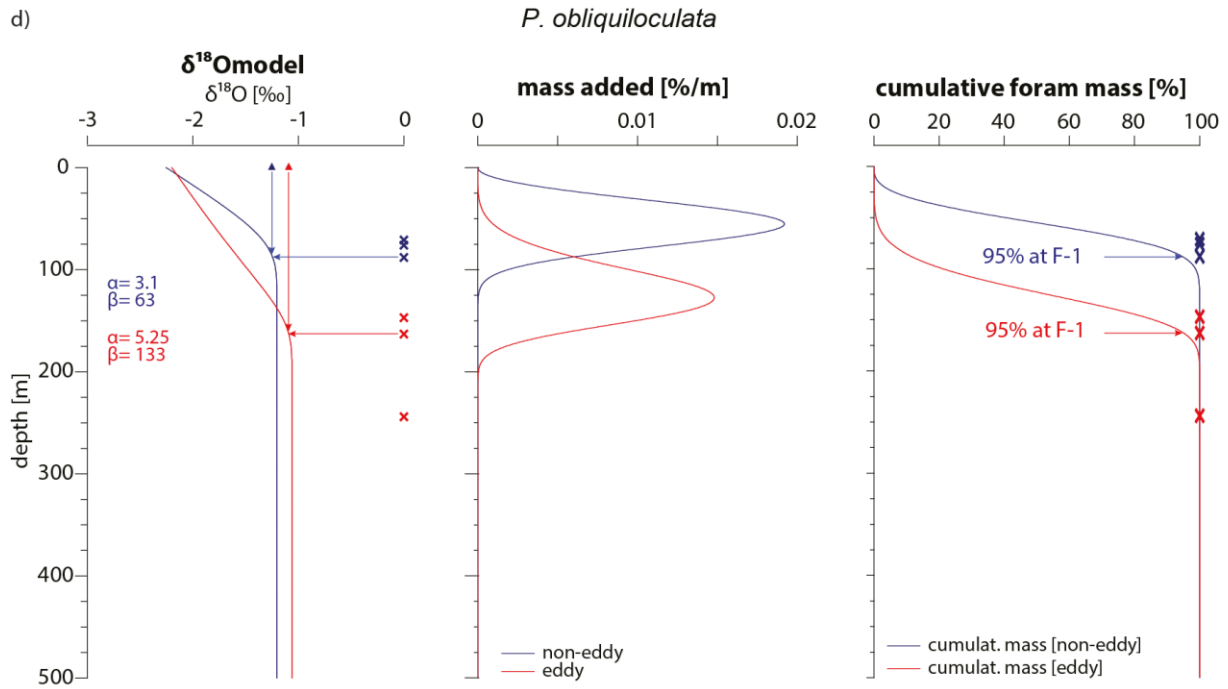


Figure 7

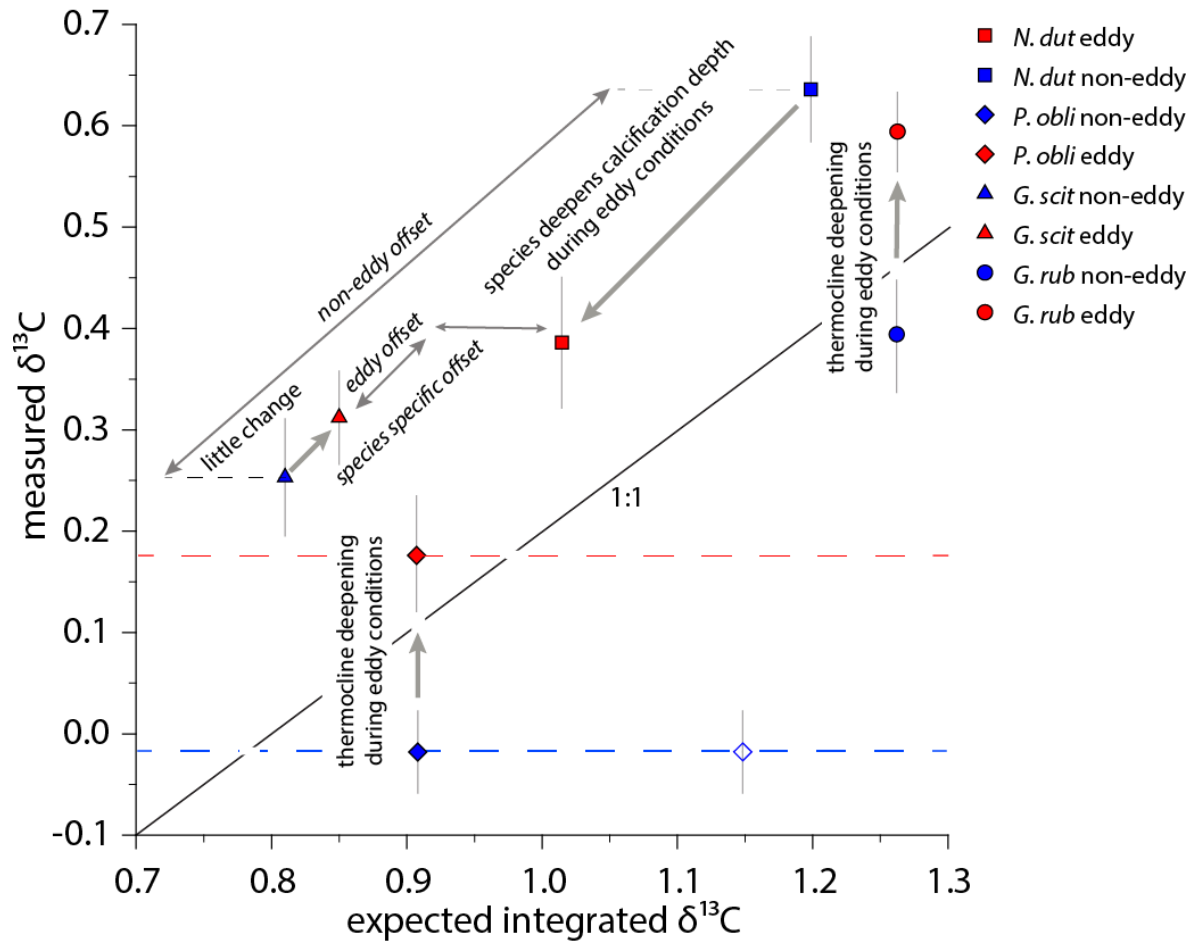


Figure 8

Figure captions:

Figure 1: Hydrography of southwestern Indian Ocean and location of the sediment trap (star) within the mooring array (right top). On the right bottom a map of sea level anomaly shows the passing of an anti-cyclonic eddy over the trap location (star). AVISO sea level anomaly map was produced using the AVISO live access server (<http://las.aviso.altimetry.fr/las/getUI.do>). EACC: East African Coastal Current, SEC: South Equatorial Current, AC: Agulhas Current.

Table 1: Average Mg/Ca ratios (Steinhardt et al., 2014), $\delta^{18}\text{O}$ and $\delta^{13}\text{C}$ with standard errors (SE) and corresponding standard deviations (SD). Mg/Ca-based temperature are based on species specific temperature equations. The equation developed by Fallet et al. (2010) was applied for *G. ruber*. The equations developed by Anand et al. (2003) were applied to *N. dutertrei*, *P. obliculata*. For *G. scitula* Anand's equation for *G. hirsuta* was applied following the example of Fallet et al. (2011). Calculate $\delta^{18}\text{O}$ -based temperatures are based on the equation of Kim and O'Neil (1997).

Table 2: Average measurements of $\delta^{18}\text{O}$ and $\delta^{13}\text{C}$ with standard errors (SE) and corresponding standard deviations (SD) performed at the Universitat Autònoma de Barcelona on a Thermo Finnigan MAT253 mass spectrometer coupled to a Kiel IV device for CO₂ sample gas preparation (BCN) and the Thermo Finnigan Delta Plus mass spectrometer equipped with a Gas Bench II preparation device at the VU University Amsterdam (VU). Measurements of *N. dutertrei*, *P. obliquiloculata* and *G. scitula* are comparable and species-specific values are in good agreement

Figure 2: Scatter plot of single shell $\delta^{13}\text{C}$ versus $\delta^{18}\text{O}$ with analytical error. Note the linear relation in *G. scitula* ($r^2=0.388$, $p<0.001$).

Figure 3: Eddy (red circles), non-eddy (blue circles) comparison of $\delta^{13}\text{C}$ PDB and $\delta^{18}\text{O}$ PDB for the analyzed species. Grey lines indicate standard deviation (SD), black capped lines are indicative of standard error (SE).

Table 3: Results for $\delta^{18}\text{O}$ and $\delta^{13}\text{C}$ with standard errors (SE) and corresponding standard deviations (SD) under eddy and non-eddy conditions for *G. ruber*, *N. dutertrei*, *P. obliquiloculata* and *G. scitula*.

Figure 4: Scatter plot of Mg/Ca versus $\delta^{18}\text{O}_{\text{cc}}$ (left panel). Right panel: single chamber Mg/Ca exponential relationship with $\delta^{18}\text{O}$ -derived Temperatures calculated using Kim & O'Neil (1997). Regression: $f = a \cdot \exp(b \cdot x)$, with $a=-0.7$, $b=0.06$, $r^2=0.47$ using F-1/2 Mg/Ca from *G. ruber*, F-0 for *N. dutertrei*, *P. obliquiloculata* and *G. scitula* (black circles). F-1 for *N. dutertrei*, *P. obliquiloculata* and *G. scitula* (red circles) and F-2 for *N. dutertrei*, *P. obliquiloculata* and *G. scitula* (blue circles). Mg/Ca data from Steinhardt et al. (2014). Note that the correlation coefficient also indicates that approximately 60% of the observed variability is not due to temperature alone.

Figure 5: Inter-species $\delta^{18}\text{O}$ - and Mg/Ca-derived temperature for eddy and non-eddy intervals. Circles: $\delta^{18}\text{O}$ -based temperatures using the equation of Kim and O'Neil (1997), Squares represent Mg/Ca-based temperatures using the species specific equations of Anand et al. (2003) for *N. dutertrei*, *P. obliquiloculata* and *G. scitula*. For *G. ruber*, the equation of Fallet et al. (2011) was used. Vertical error bars (SD) for $\delta^{18}\text{O}$ derived temperatures, horizontal error bars (SD) for Mg/Ca derived temperatures. Red colors: *G. ruber*, blue: *N. dutertrei*, orange: *P. obliquiloculata*, green: *G. scitula*.

Figure 6: Apparent calcification depths of species are generally shallower during non-eddy conditions. Apparent calcification depths for eddy (red) and non-eddy conditions (blue) calculated from single specimen $\delta^{18}\text{O}_{\text{cc}}$ using *in situ* temperature and $\delta^{18}\text{O}_{\text{w}}$. Calcification depth was determined by matching the measured foraminiferal $\delta^{18}\text{O}_{\text{cc}}$ with the $\delta^{18}\text{O}_{\text{eq}}$, using the equation of Kim and O'Neil (1997). We used $\delta^{18}\text{O}_{\text{sw}}$ from the species calcification depth. Grey box indicates the zone of the close-up on the right (upper 200 m).

Figure 7: Cumulative calcification model for eddy (red) and non-eddy (blue) conditions from left to right: temperature profiles as well as $\delta^{18}\text{O}_{\text{equilibrium}}$ ($\delta^{18}\text{O}_{\text{eq}}$) for the upper 1000 m and $\delta^{18}\text{O}_{\text{cumulative}}$ ($\delta^{18}\text{O}_{\text{model}}$) for the upper 500m (a). On the upper far right, mass development/growth pattern, below cumulative mass of the foraminifera (foram mass) is plotted for the upper 500 m. Bulk $\delta^{18}\text{O}_{\text{foram}}$

(triangles) Mg/Ca derived single chamber calcification depth (crosses) are indicated in the relevant plots for *G. ruber* (b), *N. dutertrei* (c), *P. obliquiloculata* (c) and *G. scitula* (d)

Figure 8: Inter-species differences between expected $\delta^{13}\text{C}$ values, based on the cumulative mass balance model, and measured $\delta^{13}\text{C}$ values of *G. ruber*, *N. dutertrei*, *P. obliquiloculata* and *G. scitula*. Dashed line indicates the 1:1 line of measured and expected $\delta^{13}\text{C}$. Red symbols represent values for eddy conditions, blue symbols represent values for non-eddy condition. Thick grey arrows indicate intra-species trends between non-eddy and eddy conditions, thin arrows indicate inter-specific trends. *P. obliquiloculata* does not calcify in isotopic equilibrium with dissolved ΣCO_2 , but the deviation from isotopic equilibrium is a linear function of temperature (Mulitza et al., 1999), hence there is no projected $\delta^{13}\text{C}_{\text{expect}}$, this is indicated by the dotted lines. Open diamond indicates $\delta^{13}\text{C}_{\text{expect}}$ for *P. obliquiloculata* non-eddy conditions.